Journal of Great Lakes Research xxx (2016) xxx–xxx

Contents lists available at ScienceDirect

Journal of Great Lakes Research

journal homepage: www.elsevier.com/locate/jglr

Variability of light absorption properties in optically complex inland waters of Lake Chaohu, China

Kun Xue [a,b], Yuchao Zhang [a], Hongtao Duan [a], Ronghua Ma [a,*]

[a] Key Laboratory of Watershed Geographic Sciences, Nanjing Institute of Geography and Limnology, Chinese Academy of Sciences, 73 East Beijing Road, Nanjing 210008, China
[b] University of Chinese Academy of Sciences, Beijing 100049, China

ARTICLE INFO

Article history:
Received 7 December 2015
Accepted 14 October 2016
Available online xxxx

Keywords:
Phytoplankton pigments
Non-algal particles (NAP)
Colored dissolved organic matter (CDOM)
Colored detrital matter (CDM)
Absorption budget
Spectral slope of absorption coefficient

ABSTRACT

Absorption coefficients of phytoplankton, colored detrital matter (CDM), non-algal particles (NAP), colored dissolved organic matter (CDOM), and their relative contributions to total non-water absorption (a_{t-w}) are essential variables for bio-optical and radiative transfer models. Light absorption properties showed large range and variability sampled at 194 stations throughout Lake Chaohu between May 2013 and April 2015. The a_{t-w} was dominated by phytoplankton absorption (a_{ph}) and NAP absorption (a_d). The contribution of CDOM absorption to a_{t-w} was lower than 30%. Phytoplankton and NAP were the primary sources of spatial and vertical variability in absorption properties. Light absorption by CDOM, though significant in magnitude, was relatively constant. CDM absorption (a_{dg}) was dominated by NAP. The spatial variation of the absorption coefficients from each of the optically active constituents were driven by several main inflow rivers in the western and middle part of Lake Chaohu. Algal blooms and bottom resuspension contributed to vertical variability as observed by phytoplankton and NAP profiles. Specific absorption of phytoplankton had significant spatial and seasonal variations without vertical variation. The spectral slope of absorption showed no significant spatial variability ($p > 0.05$). Variations of absorption affected different ranges of remote sensing reflectance (R_{rs}) spectrum, thereby increasing the difficulty of applying the remote sensing algorithm in optically complex waters. Parameters and relationships presented in this study provide useful information for bio-optical models and remote sensing of lakes similar to Lake Chaohu in terms of optical properties.

Introduction

Inherent optical properties (IOPs, Table 1) of a water column depend on the concentration, composition, and size of optically active constituents (OACs), including phytoplankton, non-algal particulates (NAP), and colored dissolved organic matter (CDOM) (Aurin et al., 2010; Bricaud et al., 2010; McKee et al., 2003; Ylöstalo et al., 2014). The light absorption coefficients of various OACs are important parameters in determining the optical variability of natural waters and their apparent optical properties (AOPs) (Bricaud et al., 2010). Absorption of colored detrital matter (CDM) plays an essential role in the carbon cycle and in the control of the penetration of UV and blue radiation in the surface ocean layers (Bricaud et al., 2012). The absorption coefficients have been related to important biogeochemical properties, such as phytoplankton biomass, chlorophyll-*a* concentration (Chl *a*) (Bricaud et al., 1998), phycocyanin concentration (Li et al., 2015), total suspended material (TSM) (Cui et al., 2013), dissolved organic carbon (DOC) (Hestir et al., 2015; Jiang et al., 2012), and particle size distribution (PSD) (Bricaud et al., 2012; Devred et al., 2011; Roy et al., 2013). Furthermore, absorption coefficients can also be related to the diffuse attenuation coefficients of downwelling irradiance (Lee, 2005).

Many previous studies focus on light absorption properties and their variability of oceanic waters (Bricaud et al., 2010; Morel and Maritorena, 2001; Naik et al., 2013) and coastal waters (Babin et al., 2003; McKee et al., 2003). Inland lakes are more optically complex than oceanic and coastal waters (Binding et al., 2008; Shi et al., 2014). In Case I waters, OACs usually co-vary with Chl *a*, and their optical properties are controlled by phytoplankton and associated constituents (Babin et al., 2003). Complex source and composition of OACs enhance the variability of optical properties of Case II waters (Wu et al., 2011). Inland lakes usually have a relatively high OAC content and diverse optical properties (Ficek et al., 2012). Riddick et al. (2015) found that the relative contributions to the absorption budget in an optically complex lake varied more widely than oceans with a greater contribution from NAP (up to 30%).

Variability of absorption coefficients could be affected by the specific absorption coefficients and spectral slope of absorption coefficients. Chl *a*-specific absorption of phytoplankton ($a_{ph}^*(\lambda)$) is an essential component for many forward radiative transfer models and remote sensing interpretation schemes (McKee et al., 2014). The observed variability in $a_{ph}^*(\lambda)$ indicates change in pigment composition or package effect. Most of the seasonal changes observed in $a_{ph}^*(\lambda)$ were driven by

* Corresponding author.
E-mail address: rhma@niglas.ac.cn (R. Ma).

http://dx.doi.org/10.1016/j.jglr.2016.10.006
0380-1330/

Table 1
Acronyms, abbreviations, symbols and units as applied in this study.

Acronyms and abbreviations	
AOPs	Apparent optical properties
CDOM	Colored dissolved organic matter
CDM	Colored detrital matter
IOPs	Inherent optical properties
N	Number of samples
NAP	Non-algal particulates
OACs	Optically active constituents
WCH	West Lake Chaohu
MCH	Middle Lake Chaohu
ECH	East Lake Chaohu

Symbols	
$a(\lambda)$	Total absorption coefficient (m^{-1}) at wavelength (λ)
$a_g(\lambda)$	Absorption by CDOM (m^{-1}) at wavelength (λ)
$a_d(\lambda)$	Absorption by NAP (m^{-1}) at wavelength (λ)
$a_{dg}(\lambda)$	Absorption by CDM (m^{-1}) at wavelength (λ)
$a_{ph}(\lambda)$	Absorption by phytoplankton (m^{-1}) at wavelength (λ)
$a_{t-w}(\lambda)$	Total absorption, with pure water component omitted, at wavelength (λ)
$a_w(\lambda)$	Absorption by pure water (m^{-1}) at wavelength (λ)
$a_x(\lambda)$	Absorption coefficient for component "x", such as a_g, a_d, a_{ph}, and a_w, at wavelength (λ)
$a^*_{ph}(\lambda)$	Chl *a*-specific absorption by phytoplankton ($m^2\ mg^{-1}$) at wavelength (λ)
$a^*_d(\lambda)$	SPIM-specific absorption by phytoplankton ($m^2\ g^{-1}$) at wavelength (λ)
Chl *a*	Chlorophyll-*a* concentration (μg/L)
Chl *a*(z)	Vertical profile of chlorophyll-*a* concentration (μg/L)
DOC	Dissolved organic carbon concentration (mg/L)
$Q^*_a(676)$	Package effect index (dimensionless)
S_d	Slope of a_d spectrum (nm^{-1})
S_g	Slope of a_g spectrum (nm^{-1})
S_{dg}	Slope of a_{dg} spectrum (nm^{-1})
SPIM	Suspended particulate inorganic matter (mg/L)

presence and concentration of certain pigments (Lorenzoni et al., 2015). Size composition and absorption variation of phytoplankton can often be related to local eutrophic state, as the average size of phytoplankton cells usually increases from oligotrophic to eutrophic waters (Ciotti et al., 2002). Variations of phytoplankton absorption could provide an alternative technique for documenting the changes in phytoplankton size distributions and thus the eutrophic state of waters (Brito et al., 2015; Le et al., 2013). Whereas absorption coefficient can be used to reflect the NAP and CDOM abundance, spectral slope of NAP and CDOM absorption (S_d, S_g, and S_{dg}) can be related to their source, nature, or composition (Blondeau-Patissier et al., 2009).

The complex optical properties of Case II waters present distinct challenges to bio-optical modeling and water color remote sensing algorithm parameterization and performance (Li et al., 2013; Mitchell and Cunningham, 2015; Organelli et al., 2016; Shi et al., 2013). Overcoming these challenges requires optical properties to be well understood in the context of driving physical and biological dynamics of a region (Aurin et al., 2010). In addition, remote sensing data are often directly interpreted using empirical algorithms based on regressions that relate the concentration of OACs to the remote sensing signal of either one spectral band or an arithmetic combination of several bands (Ylöstalo et al., 2014). These empirical algorithms do not consider spatial and seasonal variations in IOPs (Odermatt et al., 2012; Sathyendranath, 2000). The vertical distribution of OACs has an important effect on the underwater light field and remote sensing reflectance (Gordon and Clark, 1980; Kutser et al., 2008; Stramska and Stramski, 2005). Absorption coefficients may exhibit corresponding vertical variation owing to the internal relations of OACs and IOPs. Accurate descriptions of the scales of variability in IOPs and specific IOPs are needed for an accurate inversion of the remote sensing signal into biogeochemical quantities and simulation of underwater light field (Campbell et al., 2010; Oubelkheir et al., 2006).

The aims of this study are (1) to describe the characteristics of the OACs (phytoplankton, NAP, CDOM, CDM) and their absorption coefficients in Lake Chaohu, China; (2) to explore the spatial, seasonal, and vertical variations of light absorption properties; and (3) to describe the impact of absorption variations on remote sensing reflectance modeling. The present study contributes to bio-optics and remote sensing of inland waters, through extensive documentation on light absorption properties of different lake regions and seasons of Lake Chaohu.

Methods

Study area

Lake Chaohu, the fifth largest freshwater lake in China, is a eutrophic shallow lake in the lower reaches of Yangtze watershed, with an area of 770 km^2 (31°25′–31°43′N, 117°17′–117°51′E, Fig. 1) and a mean depth of 3.0 m (Chen et al., 2013; Tang et al., 2015). The area of the lake is characterized by a subtropical monsoon climate with an annual mean temperature of 15 °C–16 °C and an annual mean rainfall of 1100 mm (Chen et al., 2013). The eight major inflowing rivers of Lake Chaohu (Fig. 1), namely, Zhegao River (ZGR), Nanfei River (NFR), Shiwuli River (SWLR), Pai River (PR), Fengle River (FLR), Hangbu River (HBR), Baishitian River (BSTR), Zhao River (ZR), account for >80% of the total inflows of the lake basin. Yuxi River is the only outflowing river as well as an influent to the Yangtze River (Fig. 1).

Lake Chaohu is the primary source of drinking water for the provincial capital Hefei City and for the medium-sized Chaohu City of Anhui province (Qin et al., 2013) (Fig. 1). >9.1 million people live in the lake watershed, where agricultural runoff, industrial pollution, and municipal sewage are the three major pollution sources (Qin et al., 2013; Yang et al., 2013).

In Lake Chaohu, water quality is poor, and algal blooms frequently occur because of severe eutrophication and pollution. Temporal and spatial changes of total nitrogen (TN), total phosphorus (TP) and Chl *a* showed no substantial improvement from 2001 to 2011 (Yang et al., 2013). The eutrophication of the western part of Lake Chaohu (WCH) is more serious than that of the middle (MCH) and eastern part (ECH) primarily because the riverine runoff is considered an important route for the transport of contaminants to Lake Chaohu (Jiang et al., 2014; Tang et al., 2015). The TN and TP content showed clear spatial variability and were significantly higher in WCH and MCH than ECH (Gao et al., 2015; Yang et al., 2013).

Data collection

Seven cruise surveys and one vertical survey, with 185 surface samples and 76 vertical samples, were performed from May 2013 to April 2015 to measure OACs and IOPs in Lake Chaohu (Fig. 1, Table 2). Water samples were collected and analyzed for the OACs and corresponding absorption coefficients. The field measurements, laboratory analysis, and data processing are briefly summarized below.

Water samples of each station were stored in the dark at a low temperature (4 °C) before laboratory analysis of chlorophyll-*a* (Chl *a*, μg/L), suspended particulate inorganic matter (SPIM, mg/L), dissolved organic carbon concentration (DOC, mg/L), and absorption coefficients (m^{-1}). Water samples of the vertical survey were obtained from nine depths (surface, 0.1, 0.2, 0.4, 0.7, 1.0, 1.5, 2.0, and 3.0 m) and collected in separate 1 L Niskin bottles using an ad hoc vertical collection device, which comprises a 3.5 m perforated tube, a small vacuum pump (0.1 m diameter), connective tubes, and a scale bar. The depth of the water inlet was controlled and determined by a scale bar (Xue et al., 2015). Wind speed were measured at each station using a FR-HW handheld anemometer (Wuhan, China).

Measurements of optically active constituents

The water samples were filtered with Whatman GF/C glass-fiber filters (pore size of 1.1 μm), and pigments were extracted using 90%

Please cite this article as: Xue, K., et al., Variability of light absorption properties in optically complex inland waters of Lake Chaohu, China, J. Great Lakes Res. (2016), http://dx.doi.org/10.1016/j.jglr.2016.10.006

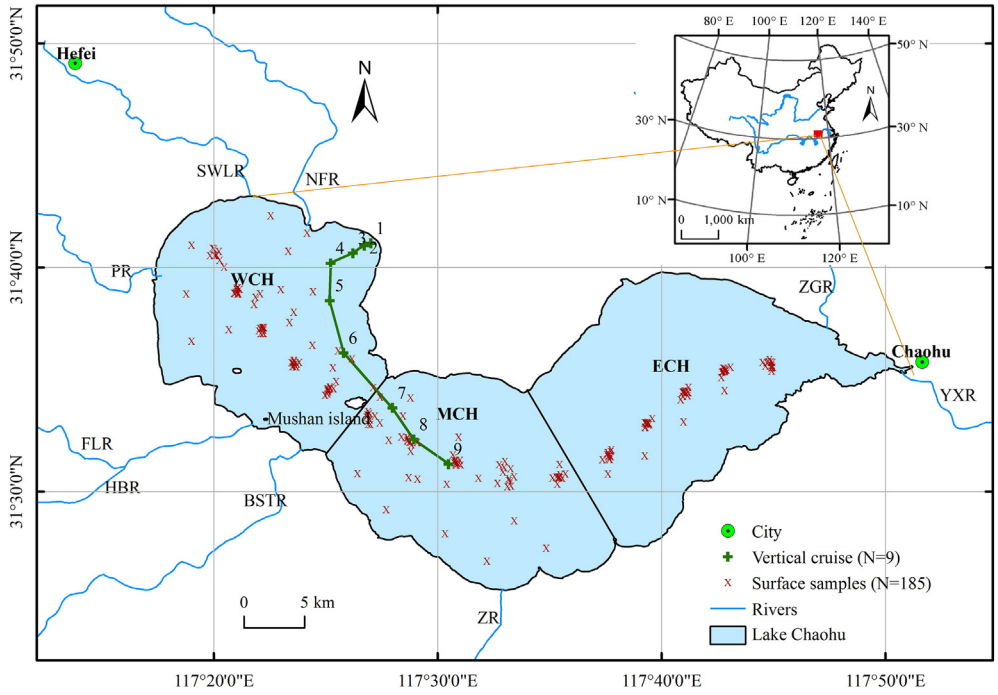

Fig. 1. Spatial distributions of the sampling stations in Lake Chaohu (symbol "X" indicates the samples collected from the water surface, and "+" indicates vertical stations). Lake Chaohu is conventionally divided into three segments separated by the dotted lines: West Lake Chaohu (WCH), Middle Lake Chaohu (MCH), and East Lake Chaohu (ECH). Several major rivers that discharge to Lake Chaohu are also annotated, including Zhegao River (ZGR), Nanfei River (NFR), Shiwuli River (SWLR), Pai River (PR), Fengle River (FLR), Hangbu River (HBR), Baishitian River (BSTR), and Zhao River (ZR). The Yuxi River (YXR) is the only outflowing river.

acetone as reference. The Chl *a* value was calculated using absorbance at 630, 645, 663, and 750 nm measured with a Shimadzu UV-2600 spectrophotometer (Werdell et al., 2013). For SPIM, 47 mm Whatman GF/F glass fiber filters were pre-combusted at 450 °C for 6 h and pre-weighted. Water samples were filtered, and filters were dried at 105 °C for 4–6 h. SPIM was derived gravimetrically by burning organic matter from the filters at 450 °C for 6 h and weighing the filters again (Jiang et al., 2012). The filtered water obtained by filtering onto pre-combusted GF/F glass fiber filters was used to determine the concentration of DOC using a Shimadzu TOC-5000A analyzer (Chen et al., 2004; Jiang et al., 2012).

Absorption coefficient

Determination of the spectral absorption coefficients of water constituents essentially involved direct measurements of three quantities, namely, absorption coefficient of phytoplankton, $a_{ph}(\lambda)$, absorption coefficient of non-algal particulates (also referred to as the detritus), $a_d(\lambda)$, and absorption coefficient of CDOM, $a_g(\lambda)$. The spectral total absorption coefficient $a(\lambda)$ was calculated as the sum of $a_{ph}(\lambda)$, $a_d(\lambda)$, $a_g(\lambda)$, and absorption coefficient of pure water, $a_w(\lambda)$.

$$a(\lambda) = a_{ph}(\lambda) + a_d(\lambda) + a_g(\lambda) + a_w(\lambda) \quad (1)$$

The absorption coefficients of pure water were obtained from Pope and Fry (1997). The methods for measurement of absorption coefficients of phytoplankton, NAP, and CDOM are described below.

Absorption coefficients of the total particulate matter, phytoplankton pigments, and NAP were determined using the quantitative filter technique (Mitchell, 1990) with 47 mm GF/F filters and a Shimadzu UV2600 spectrophotometer with 1 nm interval in the range 350 to 800 nm. Absorbance spectra of non-algal particles were measured after the pigments were bleached with sodium hypochlorite (Ferrari and Tassan, 1999). The baseline was corrected using a blank filter wetted with filtered water (Ma et al., 2006). Absorbance spectra were corrected for background by subtracting the average absorbance at 750 nm from the entire spectra (Ma et al., 2006; Zhang et al., 2007) and pathlength amplification (Cleveland and Weidemann, 1993; Ylöstalo et al., 2014). The increase in pathlength caused by multiple scattering was corrected using Eq. (2) from Cleveland and Weidemann (1993).

$$A = 0.378OD_f + 0.523OD_f^2, OD_f \leq 0.4 \quad (2)$$

where $A(\lambda)$ is the absorbance at wavelength λ and OD_f is optical density of total particulate matter on the filter. After these corrections, the

Table 2
Summary of Lake Chaohu bio-optical measurements from May 2013 (301305) to April 2015 (201504). WCH, MCH, and ECH stand for West Lake Chaohu, Middle Lake Chaohu, East Lake Chaohu, respectively. In each cruise, "S" indicates samples of water surface at 0–0.4 m; and "V" indicates vertical measurements (0, 0.1, 0.2, 0.4, 0.7, 1.0, 1.5, 2.0, 3.0 m).

Cruises	Date	N	Wind speed (m/s)	Location	Season
201305-S	May 11–14, 2013	47	1.83[a]	WCH, MCH, ECH	Spring
201305-V	May 28, 2013	76	1.09	WCH, MCH	Spring
201306-S	June 14–15, 2013	24	2.34	WCH, MCH, ECH	Summer
201309-S	September 4, 6 and 17, 2013	31	2.47	WCH, MCH, ECH	Autumn
201406-S	June 12, 2014	15	1.69	WCH, MCH, ECH	Summer
201409-S	September 20–21, 2014	24	1.66	WCH, MCH, ECH	Autumn
201501-S	January 16–17, 2015	30	2.6	WCH, MCH, ECH	Winter
201504-S	April 14, 2015	14	1.86	WCH, MCH, ECH	Spring

[a] Represents that wind speed of May 11–14 2013 was collected from historic data of nearby weather station.

Please cite this article as: Xue, K., et al., Variability of light absorption properties in optically complex inland waters of Lake Chaohu, China, J. Great Lakes Res. (2016), http://dx.doi.org/10.1016/j.jglr.2016.10.006

absorbance values were converted to absorption coefficients of total particles $a_p(\lambda)$ and NAP $a_d(\lambda)$ (m^{-1}) as follows (Cleveland and Weidemann, 1993):

$$a_i(\lambda) = 2.303 \times A(\lambda) \times A_f / V \quad (3)$$

where i represents the phytoplankton pigment or NAP, A_f is the effective filtration area, and V is the filtration volume. Absorption of phytoplankton $a_{ph}(\lambda)$ was obtained by subtracting $a_d(\lambda)$ from $a_p(\lambda)$.

CDOM absorption spectra ($a_g(\lambda)$) ranged from 280 to 700 nm with 1 nm interval and was determined from filtered water (Millipore filter with 0.22 μm pore size) using a spectrophotometer (Shimadzu UV2600) with Milli-Q water as the reference. A quartz cuvette with a light path of 1 cm was used for measurements. Absorbance at each wavelength were baseline corrected by subtracting the absorbance at 700 nm according to Eq. (5) (Bricaud et al., 1981; Ma et al., 2006; Zhou et al., 2015). The measured absorbance values were converted to absorption coefficients $a_g(\lambda)$ (m^{-1}) using the following equations:

$$a_g'(\lambda) = 2.303 \times A(\lambda)/l \quad (4)$$

$$a_g(\lambda) = a_g'(\lambda) - a_g'(700) \times \frac{\lambda}{700} \quad (5)$$

where $a_g'(\lambda)$ and $a_g(\lambda)$ are the pre-corrected and corrected absorption coefficient, respectively. $A(\lambda)$ is the absorbance at wavelength λ (nm), and l is the path length of the quartz cell (m).

Remote sensing reflectance

Following NASA protocols (Mueller et al., 2003), an ASD field spectrometer (FieldSpec Pro Dual VNIR, Analytical Spectra Devices, Inc.) was used to measure downwelling radiance and upwelling total radiance above water surface. This instrument had a spectral range of 350–1050 nm with two probes and a viewing field of 25°. The total water leaving radiance (L_{sw}), radiance of gray panel (L_p), and sky radiance (L_{sky}) were measured.

Each water spectrum was sampled at 90° azimuth with respect to the sun and with a nadir viewing angle of 45°. $L_{sw}(\lambda)$ was measured using the target probe at approximately 0.5 m above the water surface, whereas another probe measured $L_{sky}(\lambda)$. The $L_p(\lambda)$ with reflectance ρ_p was used to determine the incident downwelling irradiance [$E_d(\lambda, 0^+)$] (Eq. (6)).

$$E_d(\lambda, 0^+) = L_p(\lambda) * \pi / \rho_p \quad (6)$$

$L_{sw}(\lambda)$ consisted of the desired water leaving radiance $L_w(\lambda)$ and $L_{sky}(\lambda)$, and was corrected by:

$$L_w(\lambda) = L_{sw}(\lambda) - \rho L_{sky}(\lambda) \quad (7)$$

The water surface reflectance factor ρ depended on sky conditions, wind speed, and solar zenith angle (Mobley, 1999). Considering the average wind speed (<5 m/s) and sky conditions (under clear sky or low cloud), it was assumed to be 0.028 based on the look up table for ρ coefficient in the article of Mobley (1999). $R_{rs}(\lambda)$ was then derived by the ratio of $L_w(\lambda)$ to incident downwelling spectral plane irradiance $E_d(\lambda, 0^+)$.

$$R_{rs}(\lambda) = L_w(\lambda) / E_d(\lambda, 0^+) \quad (8)$$

Data analysis

Absorption coefficient

Bio-optical models generally combine CDOM and detrital particles into colored detrital matter (CDM) because of their similar spectral signatures. CDM absorption (a_{dg}) is the sum of NAP and CDOM absorption:

$$a_{dg}(\lambda) = a_d(\lambda) + a_g(\lambda) \quad (9)$$

Chl *a*-specific absorption coefficient of phytoplankton ($a_{ph}^*(\lambda)$) was calculated by normalizing $a_{ph}(\lambda)$ to Chl *a*. SPIM-specific absorption coefficient of NAP ($a_d^*(\lambda)$) was calculated by normalizing $a_d(\lambda)$ to SPIM.

The slope coefficient of CDOM absorption S_g (nm^{-1}) was obtained by fitting an exponential equation over the 400–700 nm wavelength range to the data via nonlinear least squares curve fitting (Ylöstalo et al., 2014) using the lsqcurvefit routine in MATLAB (R2012b) software. The $a_d(\lambda)$ spectra were similar to those of CDOM. The following expressions were fit to the spectra:

$$a_g(\lambda) = a_g(\lambda_0) \exp[S_g(\lambda_0 - \lambda)] \quad (10)$$

$$a_d(\lambda) = a_d(\lambda_0) \exp[S_d(\lambda_0 - \lambda)] \quad (11)$$

$$a_{dg}(\lambda) = a_{dg}(\lambda_0) \exp[S_{dg}(\lambda_0 - \lambda)] \quad (12)$$

where λ_0 (nm) was the reference wavelength (commonly 440 nm), $a_g(\lambda)$, $a_d(\lambda)$ and $a_{dg}(\lambda)$ was the absorption coefficient of CDOM, NAP and CDM at λ nm, and S_g, S_d, S_{dg} was the spectral slope of the $a_g(\lambda)$, $a_d(\lambda)$, and $a_{dg}(\lambda)$ spectrum, respectively.

Absorption budget

The absorption budget was presented to analyze the dominant constituent/s in the total light absorption across the visible spectrum (Naik et al., 2011), which was made by phytoplankton pigments, NAP and CDOM to the total non-water absorption coefficient (a_{t-w}). It was derived at any wavelength by:

$$a_i\%(\lambda) = a_i(\lambda) / a_{t-w}(\lambda) \times 100\% \quad (13)$$

where $a_i\%(\lambda)$ was a relative contribution of a_i to the total non-water absorption at λ nm, λ was the wavelength, i represented phytoplankton, NAP, or CDOM, and $a_{t-w}(\lambda)$ was the sum of $a_{ph}(\lambda)$, $a_d(\lambda)$ and $a_g(\lambda)$. The sample can then be optically characterized by a single point on a triangular plot, in which the axes were the fractional contributions due to each of the three components (Sathyendranath, 2000). To examine the relative contributions of phytoplankton, NAP, and CDOM absorption coefficients to the total non-water absorption, the coefficients were displayed on a normalized ternary plot at three wavebands (443, 555, and 675 nm).

According to the classification scheme of IOCCG Report 3 (Sathyendranath, 2000), seven distinct dominant types of water were identified, such as cases where only one component dominates (a_{ph}, a_d, a_g), cases where two substances dominate, and third component plays a minor role (a_{ph}-a_d, a_{ph}-a_g, a_d-a_g), and case where all the three components play important roles (a_{ph}-a_d-a_g).

Statistical analyses

The variability of each optical parameter was examined by calculating the mean, maximum, and minimum values with the standard deviations (SDs) and variation coefficients (CV = SD/mean). The relational equations between optical parameters and r^2 value of the regressions were shown in their respective figure panels. When one variable between different regions or seasons was compared, ANOVA (analysis of variance) p value was given to show whether the difference was significant or not. The F-value was used for comparing the factors of the total deviation. The number of degrees of freedom (DF) was the number of values in the calculation of a statistic that are free to vary.

Please cite this article as: Xue, K., et al., Variability of light absorption properties in optically complex inland waters of Lake Chaohu, China, J. Great Lakes Res. (2016), http://dx.doi.org/10.1016/j.jglr.2016.10.006

Modeling of remote sensing reflectance

$R_{rs}(\lambda)$ was usually modeled through IOPs according to the following equation (Gordon et al., 1988; Ma et al., 2006):

$$R_{rs}(\lambda) = f' \frac{b_b(\lambda)}{a(\lambda) + b_b(\lambda)}, \quad (14)$$

where $f' = f / Q$, f and Q varied with the illumination conditions. f' was usually set as 0.0945 (Gordon et al., 1988) and 0.0922 (Lee et al., 1998; Morel and Gentili, 1991); $a(\lambda)$ was the total absorption coefficient, calculated from Eq. (1); $b_b(\lambda)$ was the backscattering coefficient. Given the lack of available field measured backscattering coefficients, an optimization method was used to calculate the backscattering coefficient spectrum and f' of each sample based on the above bio-optical model (Ma et al., 2008).

The impact of absorption coefficients on remote sensing reflectance modeling was assessed by changing the absorption coefficient of each OAC and keeping $b_b(\lambda)$ and f' fixed. The influence of absorption variation of phytoplankton, NAP, and CDOM on $R_{rs}(\lambda)$ was estimated using Eq. (15):

$$R_{rs-M}(\lambda) = f' \frac{b_b(\lambda)}{a(\lambda) + x \cdot a_i(\lambda) + b_b(\lambda)} \quad (15)$$

x was set as ±30% or ±50% and $a_i(\lambda)$ represented $a_{ph}(\lambda)$, $a_d(\lambda)$, or $a_g(\lambda)$. The relative change between R_{rs} and modeled R_{rs-M} was calculated by:

$$\Delta R_{rs}(\lambda) = \frac{R_{rs-M}(\lambda) - R_{rs}(\lambda)}{R_{rs}(\lambda)} \times 100\% \quad (16)$$

Results

Optically active constituents

There was a great variability in concentrations of OACs (Chl *a*, SPIM, and DOC), ranging more than one order of magnitude (Tables 3–4). Chl *a* ranged from 6.85 to 138.55 μg/L with an average of 38.3 (± 29.46, N = 185) μg/L. Large dynamic ranges and high variability were also observed for SPIM (2–105, 32.32 ± 21.34 mg/L, N = 185) and DOC (0.18–22.49, 9.92 ± 4.43 μg/L, N = 185). Shi et al. (2013) reported that the average Chl *a* and SPIM of Lake Chaohu was 58.22 μg/L (23.82–165.76 μg/L) and 30.7 mg/L (8.45–68.4 mg/L), respectively.

Mean concentrations of Chl *a*, SPIM, and DOC generally decreased from WCH to MCH and ECH of Lake Chaohu (Table 3). ANOVA tests indicated significant spatial differences in Chl *a* (DF = 184, F = 25.68, $p < 0.001$) for the three segments of Lake Chaohu. Unlike Chl *a*, no significant regional variability was observed in SPIM (DF = 184, F = 1.07, $p = 0.35$) and DOC (DF = 184, F = 1.32, $p = 0.24$) for the three segments. Some seasonal differences were found for optically active constituents. In summer and autumn, concentrations of Chl *a* and SPIM were higher than that in spring (Table 4). However, average Chl *a* (54.36 ± 36.89 μg/L) and DOC (14.22 ± 1.88 μg/L) were high, and SPIM (17.27 ± 9.15 mg/L) was low in winter (only one cruise on January 16–17, 2015, Table 2). As algal blooms were recorded on January 16–17, 2015, data of one cruise might not represent the general condition of winter. More field data need to be collected to describe the temporal variation of absorption properties effectively.

Table 3
Statistics for range (first line for each parameter) and mean and standard deviation (second line) for chlorophyll-*a* concentration [Chl *a*, μg/L], suspended particulate inorganic matter [SPIM, mg/L], dissolved organic carbon [DOC, μg/L], phytoplankton absorption coefficients at 443 nm [$a_{ph}(443)$, m^{-1}] and 675 nm [$a_{ph}(675)$, m^{-1}], detrital, CDOM and CDM absorption coefficient at 443 nm [$a_d(443)$, $a_g(443)$, and $a_{dg}(443)$, m^{-1}] of Lake Chaohu from 7-cruise surveys between 2013 and 2015. WCH, MCH, and ECH stand for West Lake Chaohu, Middle Lake Chaohu, East Lake Chaohu, respectively (Fig. 1). Note: The samples with floating algae were deleted in this study, considering that their extremely high Chl *a* concentration may increase the average value dramatically.

	CH (N = 185)	WCH (N = 59)	MCH (N = 67)	ECH (N = 59)
Chl *a*	6.85–138.55	6.85–138.55	8.19–135.39	10.91–108.33
	38.3 ± 29.46	58.35 ± 36.89	30.71 ± 19.71	26.98 ± 18.76
SPIM	2–105	4–105	2–86	6–65
	30.79 ± 20	33.94 ± 24.43	29.95 ± 17.78	28.47 ± 17.1
DOC	0.18–19.94	0.21–19.94	0.19–17	0.18–15.22
	9.88 ± 4.38	10.7 ± 4.96	9.52 ± 4.02	9.4 ± 4.09
$a_{ph}(443)$	0.3–8.89	0.47–8.89	0.32–3.88	0.3–3.36
	1.25 ± 1.06	1.74 ± 1.56	1.08 ± 0.66	0.96 ± 0.53
$a_{ph}(675)$	0.16–5.39	0.17–5.39	0.16–2.1	0.23–1.89
	0.68 ± 0.62	0.97 ± 0.96	0.56 ± 0.32	0.52 ± 0.28
$a_d(443)$	0.76–7.33	0.91–6.98	1.16–-7.33	0.76–3.63
	2.4 ± 1.01	2.64 ± 1.12	2.5 ± 1.06	2.06 ± 0.71
$a_g(443)$	0.16–4.26	0.2–3.21	0.16–4.26	0.23–1.53
	0.82 ± 0.5	0.98 ± 0.54	0.79 ± 0.57	0.7 ± 0.29
$a_{dg}(443)$	1.46–8.73	1.67–8.43	1.48–8.73	1.46–4.96
	3.22 ± 1.24	3.62 ± 1.35	3.29 ± 1.34	2.75 ± 0.79

Table 4
Statistics for range (first line for each parameter) and mean and standard deviation (second line) for chlorophyll-*a* concentration [Chl *a*, μg/L], suspended particulate inorganic matter [SPIM, mg/L], dissolved organic carbon [DOC, μg/L], phytoplankton absorption coefficients at 443 nm [$a_{ph}(443)$, m^{-1}] and 675 nm [$a_{ph}(675)$, m^{-1}], detrital, CDOM absorption coefficient at 443 nm [$a_d(443)$, $a_g(443)$, m^{-1}], chlorophyll-specific phytoplankton absorption coefficients at 443 and 675 nm [$a^*_{ph}(443)$, $a^*_{ph}(675)$, $m^2\ mg^{-1}$], SPIM-specific detrital absorption coefficients at 443 nm [$a^*_d(443)$, $m^2\ g^{-1}$], and spectral slopes of detrital, and CDOM absorption (S_d, S_g, nm^{-1}) of different seasons of Lake Chaohu from 7-cruise surveys between 2013 and 2015.

	Spring (N = 61)	Summer (N = 39)	Autumn (N = 55)	Winter (N = 30)
Chl *a*	6.85–135.39	11.01–137.72	16.63–137.77	17.86–138.55
	25.15 ± 22.64	38.65 ± 30.9	44.11 ± 24.82	54.36 ± 36.89
SPIM	2–105	6–62	11–90	6–55
	28.58 ± 23.45	34.43 ± 12.6	40.59 ± 20.09	17.27 ± 9.15
DOC	0.18–19.94	11.82–15.63	4.22–14	11.84–18.29
	8.92 ± 5.27	13.29 ± 1.23	7.57 ± 1.74	14.22 ± 1.88
$a_{ph}(443)$	0.32–3.88	0.3–4.29	0.5–8.89	0.89–5.5
	0.85 ± 0.53	1.01 ± 0.73	1.32 ± 1.24	2.27 ± 1.25
$a_{ph}(675)$	0.16–2.1	0.23–2.37	0.24–5.39	0.49–3.27
	0.44 ± 0.28	0.58 ± 0.4	0.7 ± 0.72	1.28 ± 0.79
$a_d(443)$	1.16–7.33	0.76–5.5	1.04–4.72	0.91–2.39
	2.54 ± 1.16	2.7 ± 1.07	2.53 ± 0.71	1.49 ± 0.39
$a_g(443)$	0.16–1.69	0.36–1.36	0.41–3.21	0.47–4.26
	0.66 ± 0.42	0.73 ± 0.21	1.02 ± 0.54	0.93 ± 0.66
$a^*_{ph}(443)$	0.008–0.102	0.011–0.065	0.008–0.072	0.032–0.083
	0.042 ± 0.02	0.031 ± 0.012	0.03 ± 0.014	0.047 ± 0.014
$a^*_{ph}(675)$	0.005–0.037	0.006–0.039	0.004–0.032	0.019–0.038
	0.021 ± 0.008	0.018 ± 0.007	0.015 ± 0.005	0.025 ± 0.004
$a^*_d(443)$	0.038–0.923	0.023–0.243	0.039–0.25	0.025–0.161
	0.149 ± 0.147	0.091 ± 0.035	0.079 ± 0.05	0.098 ± 0.03
S_d	0.012–0.014	0.012–0.016	0.011–0.014	0.012–0.015
	0.013 ± 0.0005	0.013 ± 0.001	0.012 ± 0.0005	0.013 ± 0.001
S_g	0.012–0.03	0.013–0.028	0.013–0.028	0.014–0.043
	0.019 ± 0.004	0.018 ± 0.003	0.019 ± 0.004	0.019 ± 0.006

Light absorption properties

Absorption coefficient of phytoplankton

The absorption spectra of phytoplankton showed that the pigments had two absorption maxima at the blue (~440 nm) and red wavelength (~675 nm) (Figs. 2a-b). Ficek et al. (2013) indicated that the blue part of the spectrum (~440 nm) is due to absorption by almost all of the main pigments contained in phytoplankton cells, and the red part (~675 nm), narrower and smaller, is due primarily to the absorption by chlorophyll-*a*, and to a lesser extent by chlorophyll-*b*. Phycocyanin (PC) has an absorption peak at ~620 nm. There were substantial variations in phytoplankton absorption of Lake Chaohu. For example, $a_{ph}(443)$ and $a_{ph}(675)$ ranged more than one order of magnitude from 0.3 to

Please cite this article as: Xue, K., et al., Variability of light absorption properties in optically complex inland waters of Lake Chaohu, China, J. Great Lakes Res. (2016), http://dx.doi.org/10.1016/j.jglr.2016.10.006

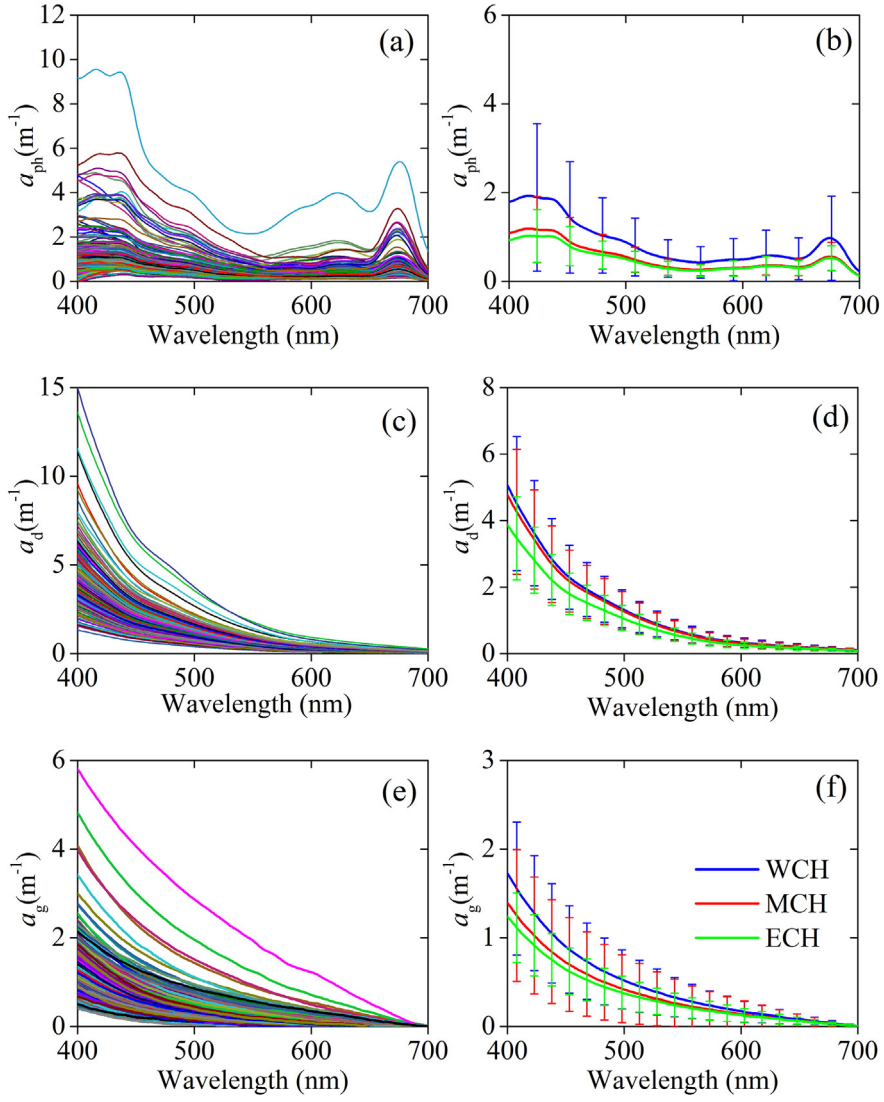

Fig. 2. Absorption spectra of (a) phytoplankton pigments ($N = 185$), (c) detrital particles ($N = 185$), (e) colored dissolved organic matter [CDOM] ($N = 185$), and (b, d, f) their mean and standard deviation of the west (WCH, $N = 59$, blue lines), middle (MCH, $N = 67$, red lines), and east (ECH, $N = 59$, green lines) parts of Lake Chaohu. (For interpretation of the references to color in this figure legend, the reader is referred to the web version of this article.)

8.89 m^{-1} and from 0.16 to 5.39 m^{-1}, respectively, corresponding to Chl *a* range of 6.85–138.55 μg/L (Table 3). The average $a_{ph}(\lambda)$ in WCH was higher than that in MCH and ECH (Fig. 2b) because of the frequent outbreak of algal blooms and high concentration of Chl *a* in WCH. Significant variability of $a_{ph}(443)$ (DF = 184, F = 10.42, $p < 0.001$) and $a_{ph}(675)$ (DF = 184, F = 10.63, $p < 0.001$) was found among the three lake segments, with average $a_{ph}(443)$ decreasing from WCH (1.74 ± 1.56 m^{-1}) to MCH (1.08 ± 0.66 m^{-1}) and ECH (0.96 ± 0.53 m^{-1}) (Table 3). In spring, $a_{ph}(443)$ ranged from 0.32 to 3.88 m^{-1} and $a_{ph}(675)$ ranged from 0.16 to 2.1 m^{-1}, while in autumn $a_{ph}(443)$ ranged from 0.5 to 8.89 m^{-1} and $a_{ph}(675)$ ranged from 0.24 to 5.39 m^{-1}. The mean $a_{ph}(443)$ were 0.85 ± 0.53 nm^{-1} and 1.32 ± 1.24 m^{-1} in spring and autumn, respectively, with significant difference (DF = 184, F = 16.28, $p < 0.001$) (Table 4).

The Chl *a*-specific phytoplankton absorption [$a^*_{ph}(443)$, $a^*_{ph}(675)$] showed large variability in Lake Chaohu (Table 5) and may pose problems when it is assumed to be constant. The variability of $a^*_{ph}(443)$ that ranged from 0.008 to 0.102 m^2 mg^{-1} with average of 0.037 ± 0.017 m^2 mg^{-1} was greater than $a^*_{ph}(675)$, ranging from 0.004 to

Table 5
Statistics for range (first line for each parameter) and mean, and standard deviation (second line) for chlorophyll-specific phytoplankton absorption coefficients at 443 and 675 nm [$a^*_{ph}(443)$, $a^*_{ph}(675)$, m^2 mg^{-1}], SPIM-specific detrital absorption coefficients at 443 nm [$a^*_d(443)$, m^2 g^{-1}], and spectral slopes of detrital, CDOM, and CDM absorption (S_d, S_g, and S_{dg}, nm^{-1}) of Lake Chaohu from 7-cruise surveys between 2013 and 2015. WCH, MCH, and ECH stand for West Lake Chaohu, Middle Lake Chaohu, and East Lake Chaohu, respectively (Fig. 1).

	CH ($N = 185$)	WCH ($N = 59$)	MCH ($N = 67$)	ECH ($N = 59$)
$a^*_{ph}(443)$	0.008–0.102	0.008–0.102	0.015–0.09	0.015–0.072
	0.037 ± 0.017	0.032 ± 0.018	0.039 ± 0.016	0.04 ± 0.015
$a^*_{ph}(675)$	0.004–0.039	0.004–0.039	0.008–0.038	0.009–0.034
	0.019 ± 0.007	0.017 ± 0.007	0.02 ± 0.007	0.022 ± 0.006
$a^*_d(443)$	0.023–0.923	0.039–0.521	0.037–0.923	0.023–0.456
	0.11 ± 0.098	0.104 ± 0.072	0.119 ± 0.129	0.106 ± 0.075
S_d	0.011–0.016	0.012–0.015	0.011–0.014	0.012–0.016
	0.013 ± 0.001	0.013 ± 0.001	0.013 ± 0.001	0.013 ± 0.001
S_g	0.012–0.043	0.014–0.028	0.012–0.03	0.012–0.043
	0.019 ± 0.004	0.02 ± 0.003	0.018 ± 0.004	0.019 ± 0.005
S_{dg}	0.012–0.017	0.012–0.016	0.012–0.017	0.012–0.017
	0.014 ± 0.001	0.014 ± 0.001	0.014 ± 0.001	0.014 ± 0.001

Please cite this article as: Xue, K., et al., Variability of light absorption properties in optically complex inland waters of Lake Chaohu, China, J. Great Lakes Res. (2016), http://dx.doi.org/10.1016/j.jglr.2016.10.006

Table 6
Bio-optical parameters (Min–Max, first line for each location, Mean ± SD, second line for each location) of several lakes or coastal waters.

Area	Chl *a* (μg/L)	SPIM (mg/L)	$a_{ph}(440)$ (m^{-1})	$a_{ph}(675)$ (m^{-1})	$a_d(440)$ (m^{-1})	$a_g(440)$ (m^{-1})	$a^*_{ph}(675)$ (m^2 mg^{-1})	$S_d(400–700)\backslash$ (nm^{-1})	$S_g(400–700)$ (nm^{-1})	Reference
Lake Chaohu	23.82–165.76	8.45–68.4	0.38–5.32	0.34–2.58	0.9–12.6	0.472–1.094	0.005–0.03	0.01–0.012	0.013–0.022	(Shi et al., 2013)
China	58.22 ± 36.61	30.7 ± 14.12	1.69 ± 1.22	0.90 ± 0.50	3.96 ± 2.14	0.682 ± 0.033	0.014 ± 0.005	0.011 ± 0.0005	0.016 ± 0.00035	$N = 32$
Lake Taihu	1.26–130.72	2.67–222.5	0.11–4.91	0.02–3.98	0.51–15.6	0.138–1.157	0.002–0.147	0.0088–0.0137	0.01–0.034	(Shi et al., 2013)
China	15	45.4	1.14	0.48	3.45	0.467	0.03	0.0112	0.017	$N = 236$
Lake Dianchi	38.97–156.7	0–22.8	1.67–5.57	0.74–2.99	0.51–3.15	0.711–2.286	0.012–0.035	0.0082–0.015	0.009–0.016	(Shi et al., 2013)
China	96.43 ± 35.76	9.01 ± 4.25	3.75 ± 1.12	2.01 ± 0.58	1.88 ± 0.73	1.657 ± 0.099	0.022 ± 0.006	0.011 ± 0.0017	0.011 ± 0.00039	$N = 25$
Lake Poyang	1.47–24.65	13–148	0.2853–2.0142	–	1.24–10.44	0.3277–1.0067	–	0.0114–0.0175	0.0096–0.0188	(Wu et al., 2011)
China	8.85 ± 6.41	48 ± 28.27	0.8008 ± 0.3057	–	4.55 ± 2.4829	0.5581 ± 0.1552	–	0.0142 ± 0.0015	0.0136 ± 0.0022	$N = 43$
Boreal lakes	1.8–94.7	–	–	–	0.04–1.78	0.43–14.5	0.008–0.020	0.0075–0.0128	0.013–0.0193	(Ylöstalo et al., 2014)
Finland	20.8	–	–	–	0.47[a]	2.65[a]	0.014	0.0101[b]	0.0164	$N = 52$
Tampa Bay	0.37–78.93	–	0.023–1.58[c]	–	0.0095–1.05[c]	0.065–9.41[c]	0.0022–0.072	0.008–0.0193	0.012–0.0192	(Le et al., 2013)
USA	7.99 ± 7.73	–	0.22 ± 0.16	–	0.19 ± 0.16	0.72 ± 1.00	0.013 ± 0.0027	0.0122 ± 0.002	0.0157 ± 0.0012	$N = 343$
Long Island Sound	0.7–80.6	–	0.008–0.478[c]	–	0.025–0.42[c]	0.12–0.75[c]	–	0.0075–0.0118	0.0109–0.0198	(Aurin et al., 2010)
USA	7.1 ± 12 ($N = 121$)	–	0.072 ± 0.126 ($N = 43$)	–	0.115 ± 0.107 ($N = 45$)	0.3 ± 0.1 ($N = 110$)	–	0.0089 ± 0.0008 ($N = 59$)	0.0147 ± 0.0014 ($N = 106$)	

[a] Represents the 442 nm wavelength.
[b] Represents the 380–700 nm.
[c] Represents the 443 nm wavelength.

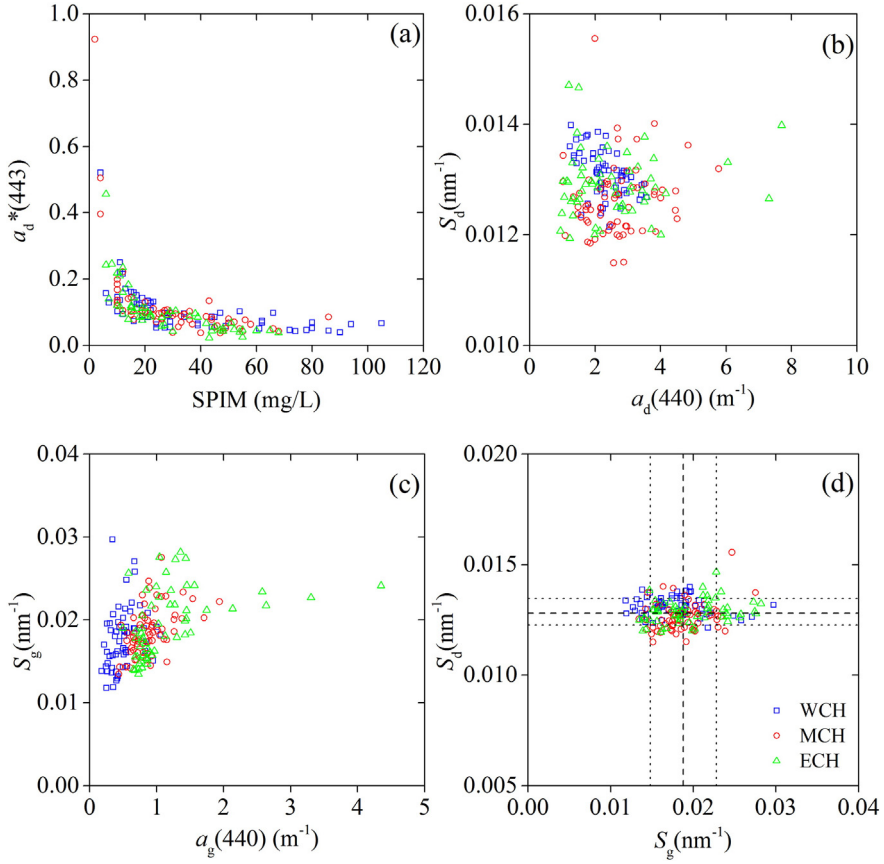

Fig. 3. Relationships between (a) suspended particulate inorganic matter [SPIM] and SPIM-specific detrital particles absorption at 443 nm [$a_d^*(443)$], (b) spectrum slope of non-algal particles absorption [S_d] and detrital particles absorption coefficient at 440 nm [$a_d(440)$], (c) spectrum slope of CDOM absorption [S_g] and CDOM absorption coefficient at 440 nm[$a_g(440)$], (d) S_d and S_g (dashed line indicates the average deviation, and dotted lines are standard deviations). WCH (blue squares, $N = 59$), MCH (red circles, $N = 67$), and ECH (green triangles, $N = 59$) stand for West Lake Chaohu, Middle Lake Chaohu, and East Lake Chaohu, respectively. (For interpretation of the references to color in this figure legend, the reader is referred to the web version of this article.)

0.039 m^2 mg^{-1} with average of 0.019 ± 0.007 m^2 mg^{-1}. $a_{ph}^*(675)$ of Lake Chaohu from May 2013 to April 2015 was comparable to the results of other studies or regions, such as Lake Chaohu, Lake Taihu, Lake Dianchi (Shi et al., 2013), and Tampa Bay (Le et al., 2013) (Table 6). In addition, significant spatial variability was observed in $a_{ph}^*(443)$ (DF = 184, F = 3.72, $p = 0.025$) and $a_{ph}^*(675)$ (DF = 184, F = 8.29, $p < 0.001$) for the three parts of Lake Chaohu. The seasonal variations of $a_{ph}^*(443)$ (DF = 184, F = 11.60, $p < 0.001$) and $a_{ph}^*(675)$ (DF = 184, F = 15.31, $p < 0.001$) were also significant. The average $a_{ph}^*(443)$ was 0.042, 0.031, 0.030, 0.047 m^2 mg^{-1} from spring to winter, and average $a_{ph}^*(675)$ was 0.021, 0.018, 0.015, 0.025 m^2 mg^{-1}, respectively (Table 4). In addition, Chl *a*-specific phytoplankton absorption coefficients of 620 nm, $a_{ph}^*(620)$, ranged from 0.0025 to 0.029 m^2 mg^{-1} with average of 0.012 ± 0.017 m^2 mg^{-1}. The average $a_{ph}^*(620)$ was 0.0138, 0.0123, 0.0109, 0.0117 m^2 mg^{-1} from spring to winter (DF = 184, F = 4.27, $p = 0.006$), and was 0.0104, 0.0126, 0.0139 m^2 mg^{-1} from WCH to ECH (DF = 184, F = 9.68, $p < 0.001$).

Absorption coefficient of NAP and CDOM

The spectral dependencies of $a_d(\lambda)$ and $a_g(\lambda)$ are both well represented by exponential functions (Eqs. (10)–(11), Fig. 2c, e). The mean $a_d(\lambda)$ and $a_g(\lambda)$ of different parts of Lake Chaohu showed that absorption of NAP is about three times that of CDOM in each part (Fig. 2d, f). Variation of $a_d(\lambda)$ was large, ranging between 0.76 and 7.33 m^{-1} at 443 nm, and $a_g(443)$ ranged more than one order of magnitude, that is, 0.16–4.26 m^{-1}. $a_{dg}(443)$ ranged from 1.46 to 8.73 m^{-1} with average value of 3.21 (±1.23) m^{-1} (Table 3). The three segments of Lake Chaohu had significant spatial variability of $a_{dg}(443)$. Higher values of

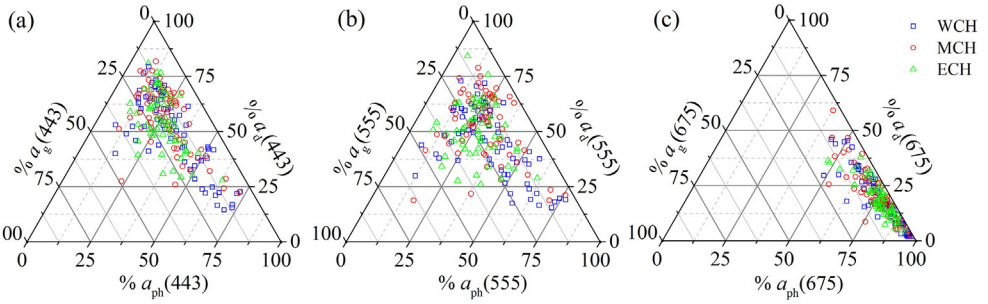

Fig. 4. Percentage contribution of phytoplankton, detrital particles, and CDOM to total non-water absorption at (a) 443 nm, (b) 555 nm, and (c) 675 nm of the water surface ($N = 185$). WCH (blue squares, $N = 59$), MCH (red circles, $N = 67$), and ECH (green triangles, $N = 59$) stand for West Lake Chaohu, Middle Lake Chaohu, and East Lake Chaohu, respectively. (For interpretation of the references to color in this figure legend, the reader is referred to the web version of this article.)

Please cite this article as: Xue, K., et al., Variability of light absorption properties in optically complex inland waters of Lake Chaohu, China, J. Great Lakes Res. (2016), http://dx.doi.org/10.1016/j.jglr.2016.10.006

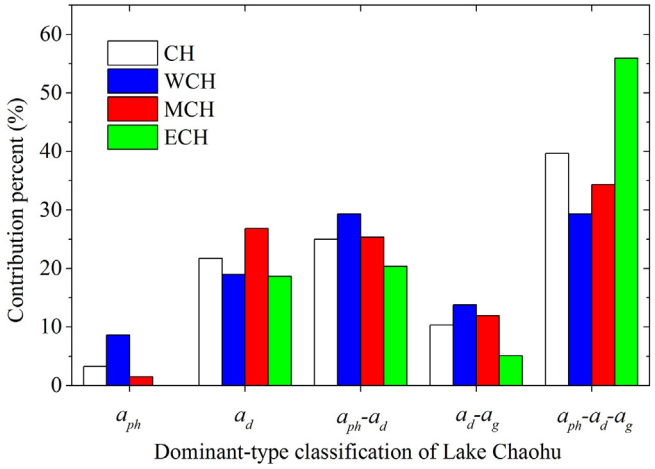

Fig. 5. Percentage of dominant types of different parts of Lake Chaohu. CH (white), WCH (blue), MCH (red), and ECH (green) stand for the Whole Lake Chaohu, West Lake Chaohu, Middle Lake Chaohu, and East Lake Chaohu, respectively. (For interpretation of the references to color in this figure legend, the reader is referred to the web version of this article.)

$a_{dg}(443)$ were found in WCH (3.62 ± 1.35 m^{-1}) and MCH (3.25 ± 1.31 m^{-1}), and the lowest average value was recorded at ECH (2.74 ± 0.79 m^{-1}) (Table 3). A significant spatial variability was also found in $a_d(443)$ (DF = 184, F = 5.61, $p = 0.004$) and $a_g(443)$ (DF = 184, F = 5.07, $p = 0.007$) with spatial trend similar to $a_{dg}(443)$. The average $a_d(443)$ were 2.54 ± 1.16 m^{-1}, 2.7 ± 1.07 m^{-1}, and 2.53 ± 0.71 m^{-1} in spring, summer, and autumn, respectively (Table 4). The average $a_g(443)$ for all 185 surface sampling sites were 0.66 ± 0.42 m^{-1} and 1.02 ± 0.54 m^{-1} in spring and autumn, respectively, with that in autumn being significantly higher than that in spring (DF = 184, F = 6.67, $p < 0.001$).

The variation of $a_d^*(\lambda)$ was large, ranging between 0.023 and 0.923 $m^2\ g^{-1}$ at 443 nm (Table 4-5, Fig. 3a). A decreasing trend of $a_d^*(443)$ is observed with increasing SPIM from 2 to 105 mg/L (Fig. 3a). $a_d^*(443)$ has no significant spatial (DF = 184, F = 0.39, $p = 0.67$) and significant seasonal (DF = 184, F = 5.63, $p = 0.001$) variability. S_d was found to vary in the range of 0.011–0.016 nm^{-1} (Table 5), with an average of 0.013 (± 0.001) nm^{-1} without significant spatial variability (DF = 184, F = 0.96, $p = 0.38$). S_d was found with significant seasonal difference (DF = 184, F = 15.88, $p < 0.001$). The average S_d of Lake Chaohu in this study was slightly higher than previous reported (Table 6). S_g varied up to fourfold from 0.012–0.043 nm^{-1}, with an overall mean of 0.019 ± 0.004 nm^{-1} ($N = 185$, Table 5). In comparison, WCH had much higher slope coefficients. However, no significant difference was found in S_g either spatially for three parts (DF = 184, F = 1.48, $p = 0.23$) or seasonally for different seasons (DF = 184, F = 0.28, $p = 0.83$). The average S_g of Lake Chaohu in this study was slightly higher than previous published (Table 6). S_{dg} showed low variation in different segments of Lake Chaohu with average of 0.014 (± 0.001) nm^{-1}, ranging from 0.012 to 0.017 nm^{-1} (Table 5). The S_d values had less variable compared with S_g (Fig. 3d), consistent with several previous studies (Table 6).

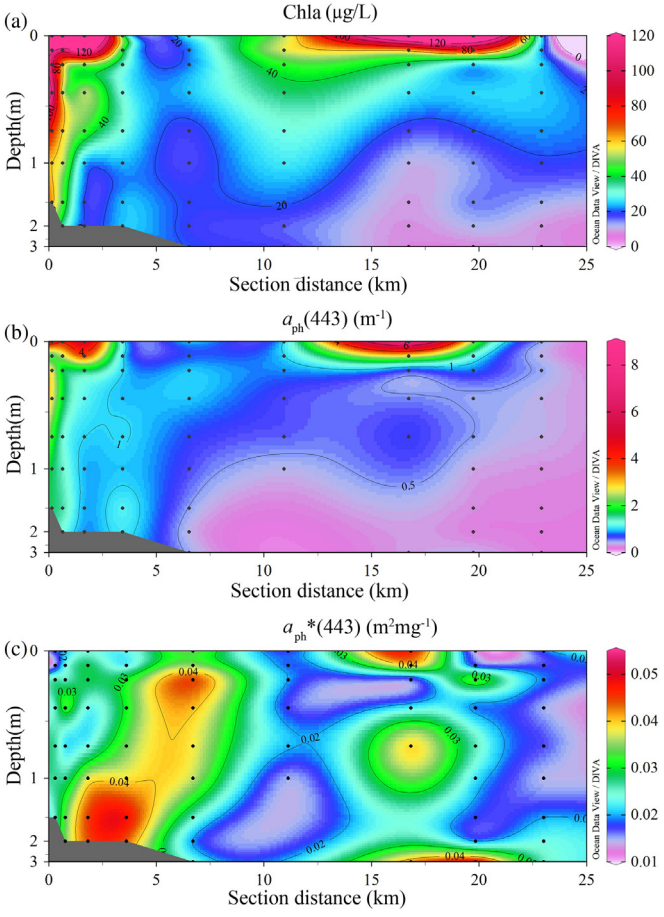

Fig. 6. Contour plots of (a) chlorophyll-*a* concentration [Chl *a*] mg m^{-3}), (b) absorption coefficient of phytoplankton at 443 nm [$a_{ph}(443)$] (m^{-1}), and (c) $a_{ph}(443)$ normalized by Chl *a* concentration [$a_{ph}^*(443)$] (m^2 mg^{-1}), for the vertical cruise transect (201305-V). Small black dots represent samples collected during the cruise.

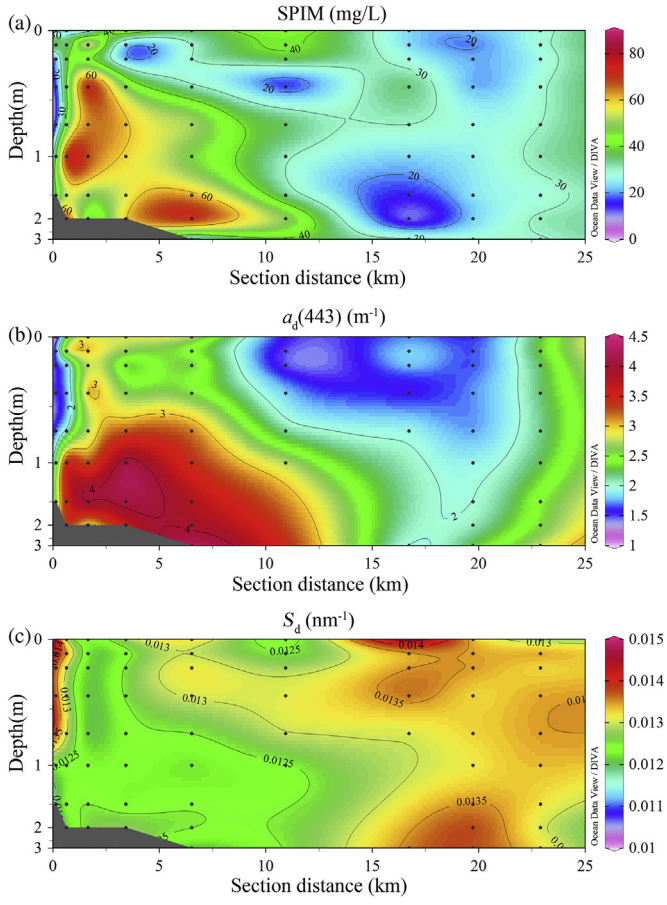

Fig. 7. Contour plots of (a) suspended particulate inorganic matter [SPIM] (mg/L), (b) the absorption coefficient of detrital particles at 443 nm [$a_d(443)$] (m^{-1}), and (c) slope of the absorption spectrum of detrital particles [S_d] (nm^{-1}), for the vertical cruise transect (201305-V). Small black dots represent samples collected during the cruise.

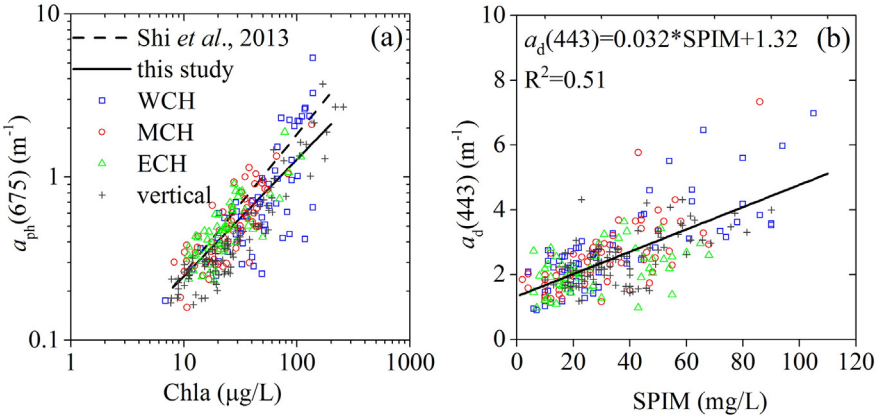

Fig. 8. Relationships of (a) chlorophyll-*a* concentration [Chl *a*] with phytoplankton absorption at 675 nm [$a_{ph}(675)$], (b) suspended particulate inorganic matter [SPIM] with detrital particles absorption at 443 nm [$a_d(443)$] ($N = 185$). Overlaid on the figures are the fitted functions of the relationships: $a_{ph}(675) = 0.0473\ \text{Chl}\ a^{0.72}$ ($r^2 = 0.63$, this study), $a_{ph}(675) = 0.0358\ \text{Chl}\ a^{0.854}$ (Shi et al., 2013). WCH (blue squares, $N = 59$), MCH (red circles, $N = 67$), and ECH (green triangles, $N = 59$) stand for West Lake Chaohu, Middle Lake Chaohu, and East Lake Chaohu, respectively. Black "+" represents vertical samples. (For interpretation of the references to color in this figure legend, the reader is referred to the web version of this article.)

Fig. 3b and c showed that S_d was plotted against $a_d(443)$, and S_g was plotted against $a_g(443)$ for three parts of Lake Chaohu. They exhibited no clear inverse relationships as suggested by previous studies (Blondeau-Patissier et al., 2009; Bricaud et al., 2010). There was no strong relationship between $a_g(443)$ and S_g (Fig. 3c) over all sites.

Dominant optical types of Lake Chaohu

The relative contributions of phytoplankton, NAP, and CDOM absorption coefficients to total non-water absorption were analyzed to determine the dominant constituent/s in the light absorption (Fig. 4). At 443 and 555 nm, $a_d(\lambda)$ and $a_{ph}(\lambda)$ dominated the total non-water absorption coefficient, while $a_g(\lambda)$ contributed <30%. At 443 nm, NAP absorption contributed most to the total non-water absorption. $a_{ph}(443)$%, $a_d(443)$%, and $a_g(443)$% were 33%, 49%, and 18% for WCH, 27%, 56%, and 17% for MCH, and 26%, 55%, and 19% for ECH, respectively. The total NAP and CDOM contribution to total non-water absorption was approximately 25% in the red region (675 nm), and the average relative contribution of $a_{ph}(675)$ was 75%.

The dominant types of the samples were derived from the classification scheme, and the results showed that type a_{ph}-a_d-a_g, which

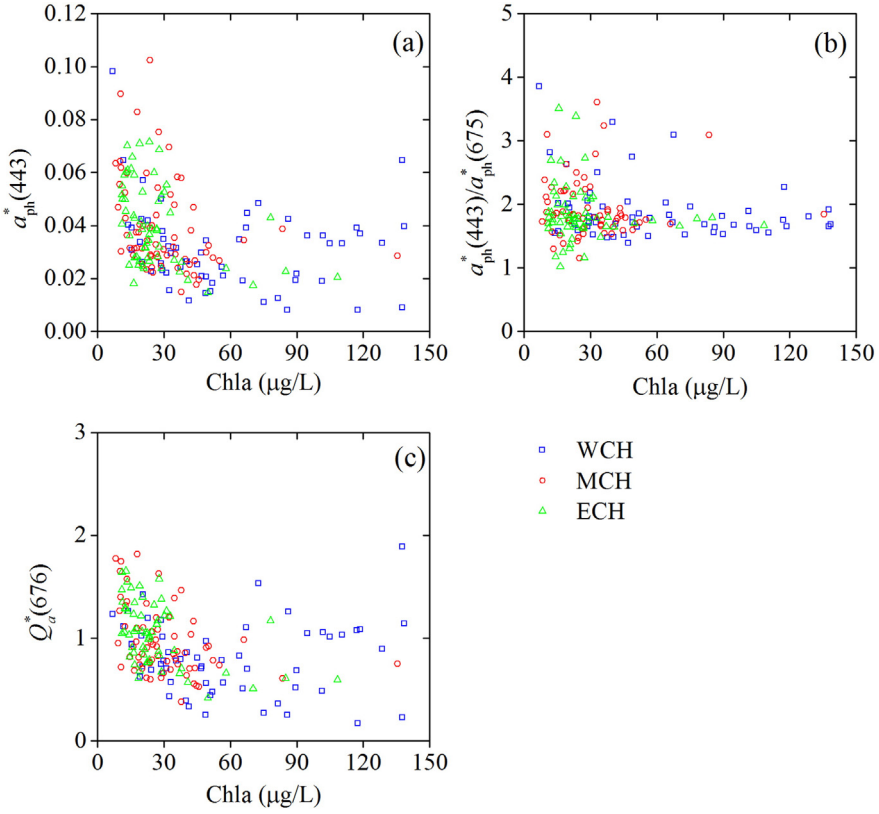

Fig. 9. Relationships of Chl *a* with (a) specific phytoplankton absorption at 443 nm [$a^*_{ph}(443)$], (b) ratio of specific phytoplankton absorption at 443 and 675 nm [$a^*_{ph}(443)/a^*_{ph}(675)$], and (c) quantification of package effect by a dimensionless factor at 676 nm [$Q^*_a(676)$]. WCH (blue squares, $N = 59$), MCH (red circles, $N = 67$), and ECH (green triangles, $N = 59$) stand for West Lake Chaohu, Middle Lake Chaohu, and East Lake Chaohu, respectively. (For interpretation of the references to color in this figure legend, the reader is referred to the web version of this article.)

Please cite this article as: Xue, K., et al., Variability of light absorption properties in optically complex inland waters of Lake Chaohu, China, J. Great Lakes Res. (2016), http://dx.doi.org/10.1016/j.jglr.2016.10.006

indicated optically complex water, played an important part in Lake Chaohu (Fig. 5). In WCH, the dominant types were a_{ph}-a_d-a_g (39.67%), a_{ph}-a_d (25%), and a_d (21.7%); type a_{ph} usually occurred in algal bloom waters. The ECH was also dominated by type of a_{ph}-a_d-a_g (55.9%), a_{ph}-a_d (20.33%), and a_d (18.64%). Overall, light absorption was dominated by a_{ph} and a_d, and contribution of a_g was lower than 30% in Lake Chaohu. A previous study of dominant optical types of Lake Chaohu obtained a_{ph}-a_d-a_g (81.82%) and a_d-a_g (18.18%) in October 2009 ($N = 11$) (Wang et al., 2013).

Vertical profiles of absorption properties

The vertical variation of absorption properties are highly variable and dependent on meteorological, biological and hydrological conditions. On short timescales (one day to several days), algal blooms and sediment resuspension played an important role in affecting the variability of phytoplankton, NAP and CDOM absorption. To assess the vertical variations of absorption coefficients, we focused our analysis on the vertical cruise on May 28, 2013.

Among the nine stations of the cruise to examine vertical structure on May 28, 2013 (Fig. 1), algal blooms occurred at five stations (S1–S3, S7–S8), and their Chl *a* vertical distribution belonged to the negative power function with maximum occurred at water surface (see Fig. 2 and Table 2 in Xue et al., 2015). The Chl *a* profiles of four other stations (S4–S6, S9) in non-algal bloom waters belong to Gaussian distribution with maximum value at water surface (see Fig. 2 and Table 2 in Xue et al., 2015). Both Chl *a* and $a_{ph}(443)$ had maximum values at the water surface for bloom conditions; these values tended to decrease with depth. This distribution mainly resulted from the vertical movement of algae in the water column and gathered at the water surface. The contour plot of $a_{ph}(443)$ of the cruise revealed a variation range that covered more than one order of magnitude (0.2–8.07 m^{-1}) (Fig. 6b) throughout the transect. Variation of $a_{ph}(443)$ was very similar to the variation of Chl *a* (Fig. 6a), which suggested covariation between $a_{ph}(443)$ and Chl *a* concentration. However, $a_{ph}^*(443)$ was not constant, ranging from 0.012 to 0.051 m^2 mg^{-1} (Fig. 6c). The average CV of $a_{ph}^*(443)$ and $a_{ph}^*(675)$ vertical profiles is 28.8% and 24.2%, respectively.

The vertical profiles of $a_d(443)$ and S_d were displayed in Fig. 7b and c. S1–S6 exhibited higher concentration of SPIM compared with S7–S9, especially near the bottom of the lake, which possibly resulted from sediment resuspension (Fig. 7a). However, the spatial pattern of $a_d(443)$ showed much less similarity with SPIM concentration, thereby suggesting a large scatter in the $a_d(443)$ versus SPIM. High values of $a_d(443)$ were observed when SPIM was >40 mg/L and low values were observed with SPIM <30 mg/L (Fig. 7b). S_d showed less variability across the transect with high values in algal bloom waters and low values in high-suspension waters.

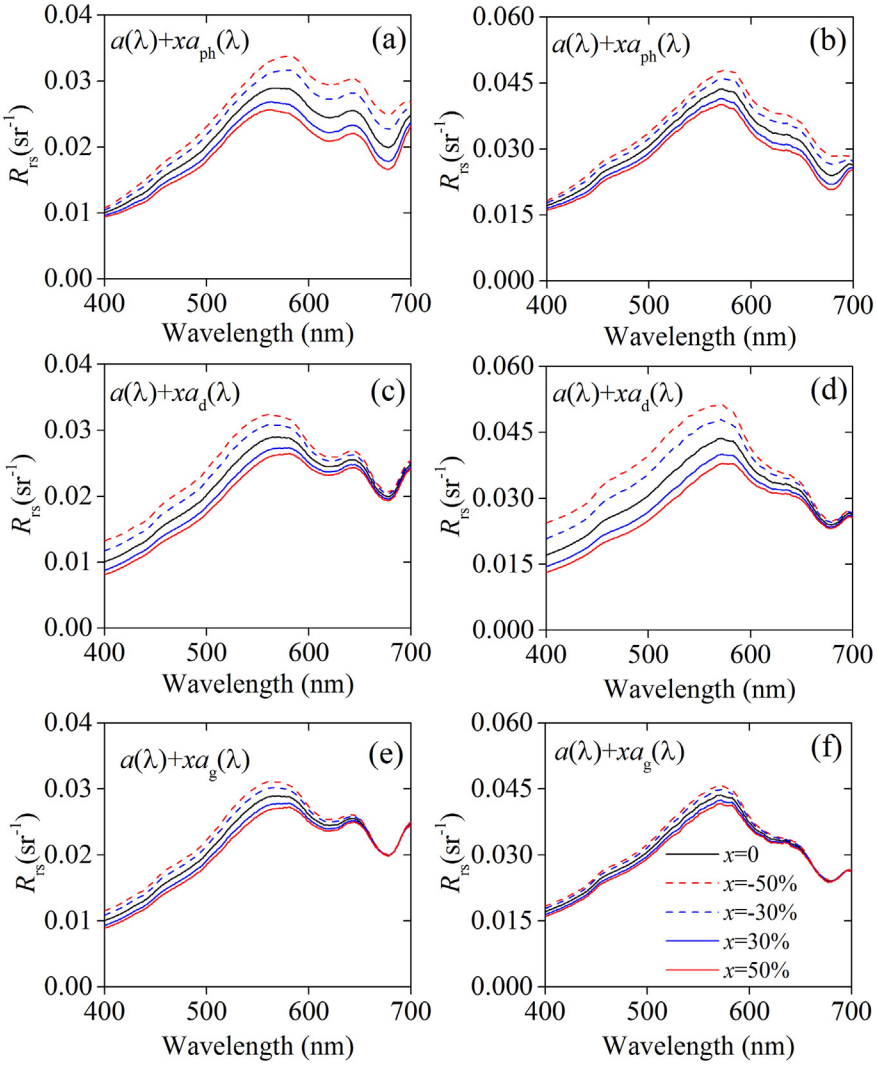

Fig. 10. Influence of (a, b) phytoplankton absorption [$a_{ph}(\lambda)$], (c, d) detrital particles absorption [$a_d(\lambda)$], and (e, f) CDOM absorption [$a_g(\lambda)$] on remote sensing reflectance [$R_{rs}(\lambda)$] modeling. N1 and N2 are two representative samples. The solid black lines are in situ $R_{rs}(\lambda)$. Sensitivity of $R_{rs}(\lambda)$ on absorption coefficient is determined by changing the $a_{ph}(\lambda)$, $a_d(\lambda)$ or $a_g(\lambda)$ value by ±30% or ±50%. (For interpretation of the references to color in this figure, the reader is referred to the web version of this article.)

Vertical structure of DOC and $a_g(443)$ of the cruise exhibited different patterns in accordance with the result of surface samples. High DOC concentration was observed at S6-S8 mainly no deeper than 0.5 m, whereas $a_g(443)$ had the highest values at S1–S2 and S6, reaching $>1.5\ m^{-1}$ in the algal bloom waters and lowest values at S7–S8. CVs of S_g covered 12% to 29.6%, showing a larger variation than S_d without a regular vertical trend.

Relationship of OACs and absorption coefficients

For the entire data range, dependence of $a_{ph}(675)$ on Chl *a* can be described using power functions ($a_{ph}(675) = 0.0473\ \text{Chl}\ a^{0.72}$, $r^2 = 0.63$) when Chl *a* varied from 6.85 to 138.55 μg/L (Fig. 8a). Similar relationships were found if the data were partitioned according to different regions. The function of $a_{ph}(675)$ and Chl *a* was slightly lower than that reported in Shi et al. (2013) ($a_{ph}(675) = 0.0358\ \text{Chl}\ a^{0.854}$, Fig. 8a). Zhang et al. (2007) provided a linear regression between $a_{ph}(675)$ and Chl *a* in Lake Taihu of China ($a_{ph}(675) = 0.0176\ \text{Chl}\ a - 0.0723$).

For NAP absorption, $a_d(443)$ increased with increasing SPIM following a linear function ($a_d(443) = 0.032\ \text{SPIM} + 1.32$, $r^2 = 0.51$, with SPIM ranging 2–102 mg/L) (Fig. 8b). No significant correlation was found between $a_g(443)$ and DOC at wavelengths of 400–700 nm at a significance level of 0.05 for the water surface samples. The results also showed no significant correlation between $a_g(443)$ and Chl *a* or SPIM, thereby further confirming the complex component of water constituents.

A decreasing trend of $a_{ph}^*(443)$ from to 0.102 to 0.008 $m^2\ mg^{-1}$ was observed with increasing Chl *a* from 6.85 to 138.55 μg/L (Fig. 9a). As the accessory pigments are known to absorb significantly higher amounts of light in the blue region than in the red, the blue to red ratio of specific absorption coefficient [$a_{ph}^*(443)/a_{ph}^*(675)$] is strongly correlated with the ratio of accessory pigments to Chl *a* (Naik, 2010). This ratio varied from 1.02 to 3.84, demonstrating an approximate fourfold decrease as Chl *a* increasing (Fig. 9b). $a_{ph}^*(676)$ variability was attributed mainly to package effect (Naik, 2010), and could be quantified by $Q_a^*(\lambda)$, which is the ratio of $a_{ph}^*(\lambda)$ and specific phytoplankton absorption of the same pigmented material in suspension [$a_{ph\,sol}^*(\lambda)$]. With $a_{ph\,sol}^*(676)$ set equal to 0.0207 $m^2\ mg^{-1}$ (Bricaud et al., 1995; Naik et al., 2011; Naik et al., 2013), $Q_a^*(676)$ was calculated. $Q_a^*(676)$ decreased from 1.89 to 0.17 with increasing Chl *a* concentration in Lake Chaohu (Fig. 9c).

Impact of absorption variations on remote sensing reflectance modeling

In order to investigate the effect of light absorption on remote sensing reflectance modeling, absorption coefficients from field measurements and backscattering coefficients derived from the optimization method were used to model remote sensing reflectance at two stations (N1, N2) (Fig. 10). Keeping $b_b(\lambda)$ the same, effect of $a_{ph}(\lambda)$ variation on the green and red wavelengths and to a lesser extent on the blue wavelengths was apparent on $R_{rs}(\lambda)$ spectra for the two samples (Fig. 10a, b). 50% variation of $a_{ph}(\lambda)$ led to about 20% relative change of $R_{rs}(\lambda)$ in the red range. The influence of $a_d(\lambda)$ variation on $R_{rs}(\lambda)$ spectra focused on the blue and green wavelengths, similar with $a_g(\lambda)$ (Fig. 10c–f). NAP absorption had a more important impact on the reflectance than CDOM absorption, about a factor of 2–3 over the blue-green domain. Effect of changing CDOM absorption became negligible compared to the effect of variability in particulate absorption. Variations of $a_{ph}(\lambda)$ and $a_{dg}(\lambda)$ affected different ranges of $R_{rs}(\lambda)$ spectrum, thereby adding to the difficulty of remote sensing algorithm application. Those empirical blue-green band-ratio based Chl *a* algorithms are unlikely to work in Lake Chaohu. Chl *a* inversion algorithm development in optically complex waters had focused on utilizing longer wavelengths. Alternatively, developing spatial or seasonal semi-analytical algorithms based on the specific absorption properties may also be feasible to avoid the absorption variation.

Discussion

Variations of light absorption coefficients

Chl a-specific absorption of phytoplankton

The observed variability in $a_{ph}^*(\lambda)$ indicated change in pigment composition or package effect. Accessory pigments are known to absorb significantly higher amounts of light in the blue region than in the red. $a_{ph}^*(443)/a_{ph}^*(675)$ showed the ratio of accessory pigments to Chl *a* (Naik, 2010). $a_{ph}^*(443)/a_{ph}^*(675)$ can also be used as an indicator of phytoplankton size, with higher values (e.g., $a_{ph}^*(443)/a_{ph}^*(675) > 3$) known to be associated with smaller cells (Naik et al., 2013). Previous studies of other regions showed that the blue to red ratio of small cells were typically >2.5 (Naik, 2010). A large part of $a_{ph}^*(443)/a_{ph}^*(675)$ values were <3 (mean = 1.92), signifying a relatively larger phytoplankton size in Lake Chaohu. Several values of $a_{ph}^*(443)/a_{ph}^*(675) > 3$ were also obtained. The inverse correlation of $a_{ph}^*(443)/a_{ph}^*(675)$ with Chl *a* indicated the dominance of smaller phytoplankton size at low Chl *a*, and vice versa (Fig. 8b). The significant seasonal and spatial variation of $a_{ph}^*(620)$ also showed the presence of phycocyanin (PC) pigments. PC absorption peaks around 610–620 nm and imparts a blue-green color in combination with Chl *a*.

Pigment packaging leads to absorption variation as phytoplankton cells accumulate in algal bloom waters. Average value of $a_{ph}^*(675)$ was lower at water surface than in the water below, which might be caused by larger *Microcystis* colonies accumulated and moved to the water surface (Zhu et al., 2014). For example, it has been reported that *Microcystis* colonies with diameters <200 μm distributed vertically homogeneously in the water column, and tended to gather in the water surface with diameters between 200 μm and 800 μm (Fan et al., 2013). $a_{ph}^*(676)$ variability was attributed mainly to package effect (Naik, 2010). Decrease of $Q_a^*(676)$ from 1.89 to 0.17 with increasing Chl *a* concentration (Fig. 8c) showed the effect of pigment packaging on $a_{ph}^*(\lambda)$ variation in Lake Chaohu.

Variation of $a_{ph}^*(\lambda)$ is also influenced by associated uncertainties in Chl *a* and $a_{ph}(\lambda)$ measurements (McKee et al., 2014). For instance, incorporating previously derived uncertainty estimates of 21% and 28% for $a_{ph}(\lambda)$ and Chl *a*, respectively, obtains an uncertainty of 33% for $a_{ph}^*(\lambda)$ (McKee et al., 2014). Incomplete removal of phytoplankton pigments through depigmentation may introduce mismatch between the desired absorption coefficients of $a_d(\lambda)$ and $a_{ph}(\lambda)$ and the actual (Binding et al., 2008; Zheng and Stramski, 2013).

CDM absorption

It has been shown that CDM is largely dominated by CDOM in global ocean (Bricaud et al., 2012; Nelson et al., 1998), but CDM of Lake Chaohu was largely dominated by NAP, for example, $a_d(443)/a_{dg}(443)$ was 74%, 70% and 78% at 443, 555 and 675 nm, respectively. There is some evidence that S_{dg} (approximately 0.010 to 0.050 nm^{-1}) is variable spatially and seasonally, both in the coastal and open ocean (Bricaud et al., 2012). S_{dg} and S_g had no significant spatial, seasonal, and vertical variability with relatively small variation. S_{dg} of Lake Chaohu had weak variation (0.012–0.017 nm^{-1}) and showed no clear inverse relationship with $a_{dg}(443)$ ($r^2 < 0.1$) ranging from 1.46 to 8.73 m^{-1}. S_{dg} variations were generally considered to reflect variations in the composition of NAP. To a lesser extent, the variable contribution of CDOM absorption to the CDM also contributed to the overall variability in S_{dg}. S_g and S_d show less vertical variability with average CV of 18.9% and 3.4%, respectively, which is lower than the CV of surface samples.

Average S_g (0.019 nm^{-1}) in Lake Chaohu was slightly higher than that in Lake Taihu, China (Shi et al., 2013), Lake Poyang, China (Wu et al., 2011), boreal lakes of southern Finland (Ylöstalo et al., 2014), Tampa Bay of the USA (Le et al., 2013), and coastal waters around Europe (Babin et al., 2003) (Table 6). Brezonik et al. (2015) reported that CV of $a_g(440)$ was 30%–50% in lakes and rivers of the U.S. Upper Midwest and lakes in Florida, and S_g in a given water body tended to have

Please cite this article as: Xue, K., et al., Variability of light absorption properties in optically complex inland waters of Lake Chaohu, China, J. Great Lakes Res. (2016), http://dx.doi.org/10.1016/j.jglr.2016.10.006

only small variations over time scales up to a decade or more. S_g showed larger variability at smaller $a_g(443)$, which is expected from the experimental random error (Babin et al., 2003). A possible explanation for the lack of correlation between $a_g(443)$ and S_g is that there are multiple sources and processes affecting the composition of the DOM pool (Hestir et al., 2015). S_g can be used as an indicator of the composition and processes acting on CDOM, and has been shown to be related with DOM composition, molecular weight of CDOM, mixing of end members, and photochemical bleaching (Blough and Del Vecchio, 2002). The weak correlation between $a_g(443)$ and Chl *a* ($r^2 < 0.1$) can be attributed to CDOM processes being out of phase with phytoplankton biomass or production, and it indicated that most CDOM of Lake Chaohu was from river input or terrestrial origin (Naik et al., 2013). The variability of S_g has also been proposed to be related to the relative importance of fulvic and humic acids (Xi et al., 2013). High S_g values measured in Lake Chaohu indicated that fulvic acids dominate the CDOM.

The S_d values were less variable compared with S_g (Fig. 3d), consistent with several previous studies (Table 6). S_d values (mean = 0.013 nm^{-1}) in Lake Chaohu were slightly higher than those in Lake Taihu, China (Shi et al., 2013), Tampa Bay of the USA (Le et al., 2013), boreal lakes of southern Finland (Ylöstalo et al., 2014), and coastal waters around Europe (Babin et al., 2003), and lower than those in Lake Poyang, China (Wu et al., 2011) (Table 6). The presence of organic particles of different natures coexisting in variable proportions within the non-algal pool may lead to variations in S_d values (Bricaud et al., 2010). The mean S_d varied minimally over broad geographic regions.

Causes of light absorption variation

OACs and their light absorptions of Lake Chaohu showed large range and significant spatial variability, and the total non-water absorption was dominated by phytoplankton and NAP (>75%). Variation of phytoplankton and NAP accounted for a large part of absorption variation. Frequently occurring algal blooms enhanced the spatial and vertical variation of Chl *a* concentration. Bottom resuspension caused by wind-driven waves in inland lakes mixed the water constituents across the water column and increased the concentration of suspended particulate matters (SPM) near the bottom. These two processes changed the composition and concentration of OACs, increased the variation of absorption coefficients, and produced a more complex underwater light field.

The occurrence of algal blooms increased the aggregation of algae, and introduced obvious vertical heterogeneity of Chl *a* and $a_{ph}(\lambda)$. In addition, algal blooms changed the specific absorption of phytoplankton as a result of the package effect. $a^*_{ph}(\lambda)$ had significant spatial variation with the average value increasing from WCH to ECH (Table 5). $a^*_{ph}(\lambda)$ showed relatively lower values near the water surface, but without significant vertical variation. The significant spatial variation of $a^*_{ph}(\lambda)$ indicated that eutrophication and algal blooms affected the composition and size of phytoplankton.

On short time scales (one day to several days), bottom resuspension caused by wind driven waves played a key role in the variation of suspended matter in shallow lake (Giardino et al., 2014). Bottom resuspension affected the vertical profile of optically active constitutes, NAP absorption, and contribution of NAP to total non-water absorption in Lake Chaohu. Sediment resuspension increased the variation of $a_d(\lambda)$ and $a^*_d(\lambda)$ of the water column. S_d, S_g, and S_{dg} showed no significant spatial and vertical variations. That is, bottom resuspension had no significant effect on variations of specific absorption of NAP and spectral slope of $a_d(\lambda)$ and $a_g(\lambda)$.

Conclusions

Absorption coefficients of phytoplankton, NAP, and CDOM measured at Lake Chaohu between May 2013 and April 2015 showed a large range and variability in accordance with OACs. OACs and their absorption coefficients had significant spatial variation, especially for phytoplankton. One possible mechanism to explain this variation was serious eutrophication of WCH and increased mixing due to several main inflowing rivers in the WCH and only one outflowing river in the ECH. Algal blooms and bottom resuspension were the main physical processes that affected the vertical variations of phytoplankton and NAP, and further altered the light absorption. The main dominant absorption budget types of Lake Chaohu were a_{ph}-a_d-a_g (40%), a_{ph}-a_d (25%), and a_d (22%). Variation of phytoplankton and NAP introduced a large part of the variation in absorption in Lake Chaohu. CDM absorption of Lake Chaohu was dominated by a_d, which differed from the global ocean. Specific absorption of phytoplankton had significant regional and seasonal variations, but no vertical variation. No significant spatial variation of specific absorption and spectral slope was observed in NAP, CDOM and CDM. Variation of a_{dg} mainly affected the blue range of $R_{rs}(\lambda)$, and 50% variation of $a_{ph}(\lambda)$ can lead to about 20% relative change of $R_{rs}(\lambda)$ in the red range.

The complex constituents of OACs and large optical absorption variability could explain the unsuitability of the bio-optical models, both empirical and semi-analytical, for Lake Chaohu. With regard to water color remote sensing, our results supported the idea that algorithms may have to be developed at regional scales to perform well in inland lakes, and acquiring source, composition, and size data of the OACs may be necessary to explain the variation of IOPs. Ultimately, laboratory studies on the optical properties of a variety of particles (various types of minerals, phytoplankton, heterotrophs, and detritus) combined with information on the type of particles present in situ and coupled with hydrodynamic-biogeochemical models will probably be the best approach for remote sensing of complex coastal systems.

Acknowledgements

The authors would like to thank the colleagues from NIGLAS (Jing Li, Min Tao, Jinghui Wu, Zhaojun Nai, Zhigang Cao, and Qichun Liang) for their help with field measurements and sample collections. Financial support was provided by the State Key Program of National Natural Science of China (Grant No. 41431176) and the National Natural Science Foundation of China (Grant No. 41471287), National High Technology Research and Development Program of China (2014AA06A509).

References

Aurin, D.A., Dierssen, H.M., Twardowski, M.S., Roesler, C.S., 2010. Optical complexity in Long Island sound and implications for coastal ocean color remote sensing. J. Geophys. Res. 115, 1487–1496.

Babin, M., Stramski, D., Ferrari, G.M., Claustre, H., Bricaud, A., Obolensky, G., Hoepffner, N., 2003. Variations in the light absorption coefficients of phytoplankton, nonalgal particles, and dissolved organic matter in coastal waters around Europe. J. Geophys. Res. 108, 1–4.

Binding, C., Jerome, J., Bukata, R., Booty, W., 2008. Spectral absorption properties of dissolved and particulate matter in Lake Erie. Remote Sens. Environ. 112, 1702–1711.

Blondeau-Patissier, D., Brando, V.E., Oubelkheir, K., Dekker, A.G., Clementson, L.A., Daniel, P., 2009. Bio-optical variability of the absorption and scattering properties of the Queensland inshore and reef waters, Australia. J. Geophys. Res. 114, 1289–1301.

Blough, N.V., Del Vecchio, R., 2002. Chapter 10 - chromophoric DOM in the coastal environment A2 - Hansell, Dennis A. In: Carlson, C.A. (Ed.), Biogeochemistry of Marine Dissolved Organic Matter. Academic Press, San Diego, pp. 509–546.

Brezonik, P.L., Olmanson, L.G., Finlay, J.C., Bauer, M.E., 2015. Factors affecting the measurement of CDOM by remote sensing of optically complex inland waters. Remote Sens. Environ. 157, 199–215.

Bricaud, A., Morel, A., Prieur, L., 1981. Absorption by dissolved organic matter of the sea (yellow substance) in the UV and visible domains 1. Limnol. Oceanogr. 26, 43–53.

Bricaud, A., Babin, M., Morel, A., Claustre, H., 1995. Variability in the chlorophyll-specific absorption coefficients of natural phytoplankton: analysis and parameterization. J. Geophys. Res. 100, 321–332.

Bricaud, A., Morel, A., Babin, M., Allali, K., Claustre, H., 1998. Variations of light absorption by suspended particles with chlorophyllaconcentration in oceanic (case 1) waters: analysis and implications for bio-optical models. J. Geophys. Res. 103, 31033.

Bricaud, A., Babin, M., Claustre, H., Ras, J., Tièche, F., 2010. Light absorption properties and absorption budget of Southeast Pacific waters. J. Geophys. Res. 115, 488–507.

Bricaud, A., Ciotti, A.M., Gentili, B., 2012. Spatial-temporal variations in phytoplankton size and colored detrital matter absorption at global and regional scales, as derived from twelve years of SeaWiFS data (1998–2009). Glob. Biogeochem. Cycles 26, 262–269.

Brito, A.C., Sá, C., Brotas, V., Brewin, R.J.W., Silva, T., Vitorino, J., Platt, T., Sathyendranath, S., 2015. Effect of phytoplankton size classes on bio-optical properties of phytoplankton in the Western Iberian coast: application of models. Remote Sens. Environ. 156, 537–550.

Campbell, G., Phinn, S.R., Daniel, P., 2010. The specific inherent optical properties of three sub-tropical and tropical water reservoirs in Queensland, Australia. Hydrobiologia 658, 233–252.

Chen, Z., Li, Y., Pan, J., 2004. Distributions of colored dissolved organic matter and dissolved organic carbon in the Pearl River Estuary, China. Cont. Shelf Res. 24, 1845–1856.

Chen, X., Yang, X., Dong, X., Liu, E., 2013. Environmental changes in Chaohu Lake (southeast, China) since the mid 20th century: the interactive impacts of nutrients, hydrology and climate. Limnologica 43, 10–17.

Ciotti, Á.M., Lewis, M.R., Cullen, J.J., 2002. Assessment of the relationships between dominant cell size in natural phytoplankton communities and the spectral shape of the absorption coefficient. Limnol. Oceanogr. 47, 404–417.

Cleveland, J.S., Weidemann, A.D., 1993. Quantifying absorption by aquatic particles: a multiple scattering correction for glass-fiber filters. Limnol. Oceanogr. 38, 1321–1327.

Cui, L., Qiu, Y., Fei, T., Liu, Y., Wu, G., 2013. Using remotely sensed suspended sediment concentration variation to improve management of Poyang Lake, China. Lake Reservoir Manage. 29, 47–60.

Devred, E., Sathyendranath, S., Stuart, V., Platt, T., 2011. A three component classification of phytoplankton absorption spectra: application to ocean-color data. Remote Sens. Environ. 115, 2255–2266.

Fan, F., Li, W., Ke, F., 2013. Spatio-temporal distribution of *Microcystis aeruginosa* colony diameters in the water source region of Chaohu City. J. Lake Sci. 25, 213–220.

Ferrari, G.M., Tassan, S., 1999. A method using chemical oxidation to remove light absorption by phytoplankton pigments. J. Phycol. 35, 1090–1098.

Ficek, D., Meler, J., Zapadka, T., Woźniak, B., Dera, J., 2012. Inherent optical properties and remote sensing reflectance of Pomeranian lakes (Poland)*. Oceanologia 54, 611–630.

Ficek, D., Dera, J., Woźniak, B., 2013. UV absorption reveals mycosporine-like amino acids (MAAs) in Tatra mountain lake phytoplankton*. Oceanologia 55, 599–609.

Gao, Y., Gao, J., Yin, H., Liu, C., Xia, T., Wang, J., Huang, Q., 2015. Remote sensing estimation of the total phosphorus concentration in a large lake using band combinations and regional multivariate statistical modeling techniques. J. Environ. Manag. 151, 33–43.

Giardino, C., Bresciani, M., Stroppiana, D., Oggioni, A., Morabito, G., 2014. Optical remote sensing of lakes: an overview on Lake Maggiore. J. Limnol. 73, 210–214.

Gordon, H.R., Clark, D.K., 1980. Remote sensing optical properties of a stratified ocean: an improved interpretation. Appl. Opt. 19, 3428–3430.

Gordon, H.R., Brown, O.B., Evans, R.H., Brown, J.W., Smith, R.C., Baker, K.S., Clark, D.K., 1988. A semianalytic radiance model of ocean color. J. Geophys. Res.-Atmos. 93, 10909–10924.

Hestir, E.L., Brando, V., Campbell, G., Dekker, A., Malthus, T., 2015. The relationship between dissolved organic matter absorption and dissolved organic carbon in reservoirs along a temperate to tropical gradient. Remote Sens. Environ. 156, 395–402.

Jiang, G., Ma, R., Loiselle, S.A., Duan, H., 2012. Optical approaches to examining the dynamics of dissolved organic carbon in optically complex inland waters. Environ. Res. Lett. 7, 034014.

Jiang, Y.-J., He, W., Liu, W.-X., Qin, N., Ouyang, H.-L., Wang, Q.-M., Kong, X.-Z., He, Q.-S., Yang, C., Yang, B., Xu, F.-L., 2014. The seasonal and spatial variations of phytoplankton community and their correlation with environmental factors in a large eutrophic Chinese lake (Lake Chaohu). Ecol. Indic. 40, 58–67.

Kutser, T., Metsamaa, L., Dekker, A.G., 2008. Influence of the vertical distribution of cyanobacteria in the water column on the remote sensing signal. Estuar. Coast. Shelf Sci. 78, 649–654.

Le, C., Hu, C., English, D., Cannizzaro, J., Chen, Z., Kovach, C., Anastasiou, C.J., Zhao, J., Carder, K.L., 2013. Inherent and apparent optical properties of the complex estuarine waters of Tampa Bay: what controls light? Estuar. Coast. Shelf Sci. 117, 54–69.

Lee, Z., 2005. Diffuse attenuation coefficient of downwelling irradiance: an evaluation of remote sensing methods. J. Geophys. Res. 110.

Lee, Z., Carder, K.L., Mobley, C.D., Steward, R.G., Patch, J.S., 1998. Hyperspectral remote sensing for shallow waters. I. A semianalytical model. Appl. Opt. 37, 6329–6338.

Li, L., Li, L., Song, K., Li, Y., Tedesco, L.P., Shi, K., Li, Z., 2013. An inversion model for deriving inherent optical properties of inland waters: establishment, validation and application. Remote Sens. Environ. 135, 150–166.

Li, L., Li, L., Song, K., 2015. Remote sensing of freshwater cyanobacteria: an extended IOP inversion model of inland waters (IIMIW) for partitioning absorption coefficient and estimating phycocyanin. Remote Sens. Environ. 157, 9–23.

Lorenzoni, L., Toro-Farmer, G., Varela, R., Guzman, L., Rojas, J., Montes, E., Muller-Karger, F., 2015. Characterization of phytoplankton variability in the Cariaco Basin using spectral absorption, taxonomic and pigment data. Remote Sens. Environ. 167, 259–268.

Ma, R., Tang, J., Dai, J., 2006. Bio-optical model with optimal parameter suitable for Taihu Lake in water colour remote sensing. Int. J. Remote Sens. 27, 4305–4328.

Ma, R., Song, Q., Li, G., Pan, D., 2008. Estimation of backscattering probability of Lake Taihu waters. J. Lake Sci. 20, 375–379.

McKee, D., Cunningham, A., Slater, J., Jones, K.J., Griffiths, C.R., 2003. Inherent and apparent optical properties in coastal waters: a study of the Clyde Sea in early summer. Estuar. Coast. Shelf Sci. 56, 369–376.

McKee, D., Röttgers, R., Neukermans, G., Calzado, V.S., Trees, C., Ampolo-Rella, M., Neil, C., Cunningham, A., 2014. Impact of measurement uncertainties on determination of chlorophyll-specific absorption coefficient for marine phytoplankton. J. Geophys. Res. Oceans 119, 9013–9025.

Mitchell, B.G., 1990. Algorithms for determining the absorption-coefficient of aquatic particulates using the Quantitative Filter Technique (Qft). Proc. SPIE-Int. Soc. Opt. Eng. 1302, 137–148.

Mitchell, C., Cunningham, A., 2015. Remote sensing of spatio-temporal relationships between the partitioned absorption coefficients of phytoplankton cells and mineral particles and euphotic zone depths in a partially mixed shelf sea. Remote Sens. Environ. 160, 193–205.

Mobley, C.D., 1999. Estimation of the remote-sensing reflectance from above-surface measurements. Appl. Opt. 38, 7442–7455.

Morel, A., Gentili, B., 1991. Diffuse reflectance of oceanic waters: its dependence on sun angle as influenced by the molecular scattering contribution. Appl. Opt. 30, 4427–4438.

Morel, A., Maritorena, S., 2001. Bio-optical properties of oceanic waters: a reappraisal. J. Geophys. Res. 106, 7163.

Mueller, J.L., McClain, G.S.F.C.R., Mueller, J., Bidigare, R., Trees, C., Balch, W., Dore, J., Drapeau, D., Karl, D., Van, L., 2003. Ocean optics protocols for satellite ocean color sensor validation, revision 5, volume V: biogeochemical and bio-optical measurements and data analysis protocols. NASA Tech. Memo. 211621, 36.

Naik, P., 2010. Assessment of particulate absorption properties in the southeastern Bering Sea from in-situ and remote sensing data. J. Appl. Remote. Sens. 4, 043561.

Naik, P., D'Sa, E.J., Grippo, M., Condrey, R., Fleeger, J., 2011. Absorption properties of shoal-dominated waters in the Atchafalaya Shelf, Louisiana, USA. Int. J. Remote Sens. 32, 4383–4406.

Naik, P., D'Sa, E.J., Gomes, H.d.R., Goés, J.I., Mouw, C.B., 2013. Light absorption properties of southeastern Bering Sea waters: analysis, parameterization and implications for remote sensing. Remote Sens. Environ. 134, 120–134.

Nelson, N., Siegel, D., Michaels, A., 1998. Seasonal dynamics of colored dissolved material in the Sargasso Sea. Deep-Sea Res. I Oceanogr. Res. Pap. 45, 931–957.

Odermatt, D., Gitelson, A., Brando, V.E., Schaepman, M., 2012. Review of constituent retrieval in optically deep and complex waters from satellite imagery. Remote Sens. Environ. 118, 116–126.

Organelli, E., Bricaud, A., Gentili, B., Antoine, D., Vellucci, V., 2016. Retrieval of colored detrital matter (CDM) light absorption coefficients in the Mediterranean Sea using field and satellite ocean color radiometry: evaluation of bio-optical inversion models. Remote Sens. Environ. 186, 297–310.

Oubelkheir, K., Clementson, L.A., Webster, I.T., Ford, P.W., Dekker, A.G., Radke, L.C., Daniel, P., 2006. Using inherent optical properties to investigate biogeochemical dynamics in a tropical macrotidal coastal system. J. Geophys. Res. Oceans 111, 520–522.

Pope, R.M., Fry, E.S., 1997. Absorption spectrum (380?700 nm) of pure water. II. Integrating cavity measurements. Appl. Opt. 36, 8710–8723.

Qin, N., He, W., Kong, X.-Z., Liu, W.-X., He, Q.-S., Yang, B., Ouyang, H.-L., Wang, Q.-M., Xu, F.-L., 2013. Atmospheric partitioning and the air–water exchange of polycyclic aromatic hydrocarbons in a large shallow Chinese lake (Lake Chaohu). Chemosphere 93, 1685–1693.

Riddick, C.A.L., Hunter, P.D., Tyler, A.N., Martinez-Vicente, V., Horváth, H., Kovács, A.W., Vörös, L., Preston, T., Présing, M., 2015. Spatial variability of absorption coefficients over a biogeochemical gradient in a large and optically complex shallow lake. J. Geophys. Res. Oceans 120, 7040–7066.

Roy, S., Sathyendranath, S., Bouman, H., Platt, T., 2013. The global distribution of phytoplankton size spectrum and size classes from their light-absorption spectra derived from satellite data. Remote Sens. Environ. 139, 185–197.

Sathyendranath, S., 2000. Reports of the International Ocean-Colour Coordinating Group. 3. IOCCG, Dartmouth, Canada, p. 140.

Shi, K., Li, Y., Li, L., Lu, H., 2013. Absorption characteristics of optically complex inland waters: implications for water optical classification. J. Geophys. Res. Biogeosci. 118, 860–874.

Shi, K., Zhang, Y., Liu, X., Wang, M., Qin, B., 2014. Remote sensing of diffuse attenuation coefficient of photosynthetically active radiation in Lake Taihu using MERIS data. Remote Sens. Environ. 140, 365–377.

Stramska, M., Stramski, D., 2005. Effects of a nonuniform vertical profile of chlorophyll concentration on remote-sensing reflectance of the ocean. Appl. Opt. 44, 1735–1747.

Tang, J., Shi, T., Wu, X., Cao, H., Li, X., Hua, R., Tang, F., Yue, Y., 2015. The occurrence and distribution of antibiotics in Lake Chaohu, China: seasonal variation, potential source and risk assessment. Chemosphere 122, 154–161.

Wang, C., Duan, H., Ma, R., Zhang, Y., 2013. Inherent optical properties of large lakes in the middle-lower reaches of the Yangtze River: I. Absorption. J. Lake Sci. 497–504.

Werdell, P.J., Franz, B.A., Bailey, S.W., Feldman, G.C., Boss, E., Brando, V.E., Dowell, M., Hirata, T., Lavender, S.J., Lee, Z., Loisel, H., Maritorena, S., Mélin, F., Moore, T.S., Smyth, T.J., Antoine, D., Devred, E., d'Andon, O.H.F., Mangin, A., 2013. Generalized ocean color inversion model for retrieving marine inherent optical properties. Appl. Opt. 52, 2019–2037.

Wu, G., Cui, L., Duan, H., Fei, T., Liu, Y., 2011. Absorption and backscattering coefficients and their relations to water constituents of Poyang Lake, China. Appl. Opt. 50, 6358–6368.

Xi, H., Larouche, P., Tang, S., Michel, C., 2013. Seasonal variability of light absorption properties and water optical constituents in Hudson Bay, Canada. J. Geophys. Res. Oceans 118, 3087–3102.

Xue, K., Zhang, Y., Duan, H., Ma, R., Loiselle, S., Zhang, M., 2015. A remote sensing approach to estimate vertical profile classes of phytoplankton in a eutrophic lake. Remote Sens. 7, 14403–14427.

Yang, L., Lei, K., Meng, W., Fu, G., Yan, W., 2013. Temporal and spatial changes in nutrients and chlorophyll-α in a shallow lake, Lake Chaohu, China: an 11-year investigation. J. Environ. Sci. 25, 1117–1123.

Ylöstalo, P., Kallio, K., Seppälä, J., 2014. Absorption properties of in-water constituents and their variation among various lake types in the boreal region. Remote Sens. Environ. 148, 190–205.

Please cite this article as: Xue, K., et al., Variability of light absorption properties in optically complex inland waters of Lake Chaohu, China, J. Great Lakes Res. (2016), http://dx.doi.org/10.1016/j.jglr.2016.10.006

Zhang, Y., Zhang, B., Wang, X., Li, J., Feng, S., Zhao, Q., Liu, M., Qin, B., 2007. A study of absorption characteristics of chromophoric dissolved organic matter and particles in Lake Taihu, China. Hydrobiologia 592, 105–120.

Zheng, G., Stramski, D., 2013. A model for partitioning the light absorption coefficient of suspended marine particles into phytoplankton and nonalgal components. J. Geophys. Res. Oceans 118, 2977–2991.

Zhou, Y., Zhang, Y., Shi, K., Niu, C., Liu, X., Duan, H., 2015. Lake Taihu, a large, shallow and eutrophic aquatic ecosystem in China serves as a sink for chromophoric dissolved organic matter. J. Great Lakes Res. 41, 597–606.

Zhu, W., Li, M., Luo, Y., Dai, X., Guo, L., Xiao, M., Huang, J., Tan, X., 2014. Vertical distribution of Microcystis colony size in Lake Taihu: its role in algal blooms. J. Great Lakes Res. 40, 949–955.

Please cite this article as: Xue, K., et al., Variability of light absorption properties in optically complex inland waters of Lake Chaohu, China, J. Great Lakes Res. (2016), http://dx.doi.org/10.1016/j.jglr.2016.10.006